

Molecular jackhammers eradicate cancer cells by vibronic-driven action

Received: 10 October 2022

Accepted: 24 October 2023

Published online: 19 December 2023

 Check for updates

Ciceron Ayala-Orozco¹✉, Diego Galvez-Aranda², Arnoldo Corona³, Jorge M. Seminario^{1,2,4}✉, Roberto Rangel¹, Jeffrey N. Myers^{1,3}✉ & James M. Tour^{1,5}✉

Through the actuation of vibronic modes in cell-membrane-associated aminocyanines, using near-infrared light, a distinct type of molecular mechanical action can be exploited to rapidly kill cells by necrosis. Vibronic-driven action (VDA) is distinct from both photodynamic therapy and photothermal therapy as its mechanical effect on the cell membrane is not abrogated by inhibitors of reactive oxygen species and it does not induce thermal killing. Subpicosecond concerted whole-molecule vibrations of VDA-induced mechanical disruption can be achieved using very low concentrations (500 nM) of aminocyanines or low doses of light (12 J cm^{-2} , 80 mW cm^{-2} for 2.5 min), resulting in complete eradication of human melanoma cells *in vitro*. Also, 50% tumour-free efficacy in mouse models for melanoma was achieved. The molecules that destroy cell membranes through VDA have been termed molecular jackhammers because they undergo concerted whole-molecule vibrations. Given that a cell is unlikely to develop resistance to such molecular mechanical forces, molecular jackhammers present an alternative modality for inducing cancer cell death.

We previously used Feringa-type unidirectional rotating molecular motors that bear a rotor and stator and can be activated by ultra-violet (UV) or visible light to open pores in cell membranes, resulting in rapid necrotic death¹. Through the 2–3 MHz unidirectional rotations in these molecular motors, the drilling action on cellular membranes develops holes in the cell, followed by blebbing and death within seconds to minutes of activation. This necrotic action is unaffected by inhibitors of radical oxygen species (ROS)². Slower versions of Feringa motors, with rotation rates in the order of 1–100 Hz, do not elicit such cell-killing action, further ruling out a thermal effect in the killing². More recently, we studied visible light-activated Dube hemithioindigo switches and motors that operate in the kilohertz regime³. Despite being too slow to mechanically kill cells, these switches promote slower apoptotic cellular death by inducing ROS⁴.

While UV and visible light penetrate only hundreds of micrometres to 1 mm through human tissue (skin, muscle and fat), the near-infrared (NIR) window of 650–900 nm, also known as the optical therapeutic window, is ideally suited for *in vivo* applications owing to minimal light absorption by haemoglobin and water coupled with substantial penetration through human tissue reaching ~10 cm (ref. 5). We have previously exploited two-photon NIR activation of Feringa-type motors to induce rapid cellular necrosis, but that technique requires large laser-generated fluxes of photons and hence the depth of penetration is shallow, ~0.5 mm, and the area of coverage is restricted to smaller-sized domains, impractical for broad clinical translation⁶. In that approach, two photons of 710 nm are required to simultaneously hit the molecule and combine via a virtual state into 355 nm energy, a low-probability and thus poorly efficient process, which then activates the rotation of the Feringa-type motor⁷. Despite great efforts to tune

¹Department of Chemistry, Rice University, Houston, TX, USA. ²Department of Chemical Engineering and Department of Electrical and Computer Engineering, Texas A&M University, College Station, TX, USA. ³Department of Head and Neck Surgery, Division of Surgery, The University of Texas MD Anderson Cancer Center, Houston, TX, USA. ⁴Department of Materials Science and Engineering, Texas A&M University, College Station, TX, USA.

⁵Department of Materials Science and NanoEngineering, NanoCarbon Center, Smalley-Curl Institute and The Rice Advanced Materials Institute, Rice University, Houston, TX, USA. ✉e-mail: ca5@rice.edu; seminario@tamu.edu; jmyers@mdanderson.org; tour@rice.edu

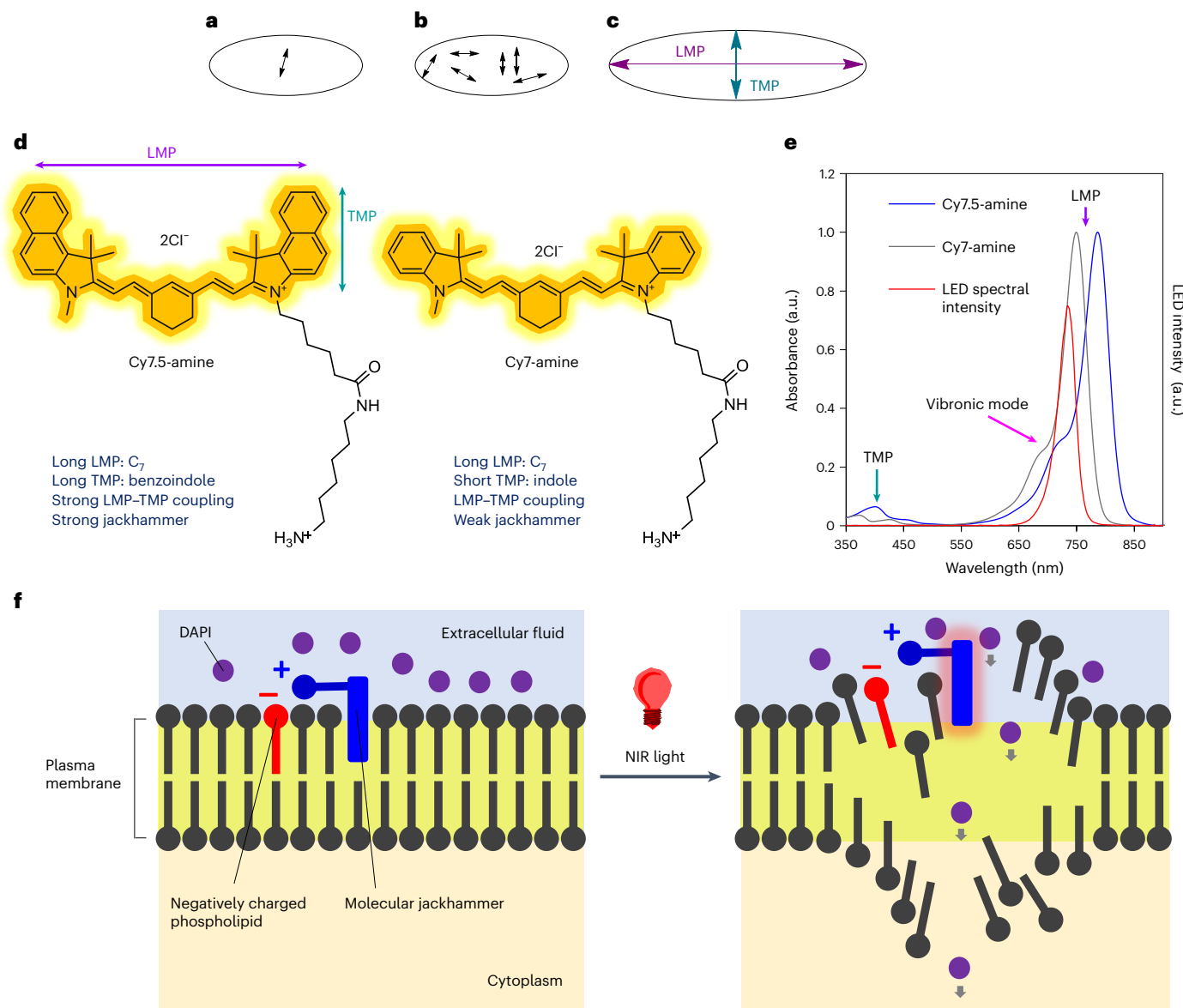


Fig. 1 | The concept of an MJH and its working mechanism. **a–c**, Schematic representation of bond vibrations, represented by arrows, induced by light excitation of a single bond (**a**), broadband light excitation of multiple bonds (**b**) and VDA for whole-molecule excitation with an LMP (purple) or TMP (teal) (**c**). **d**, Chemical structures of Cy7.5-amine and Cy7-amine. The expected molecular plasmon modes TMP and LMP are indicated. Listed below are their structural features and translated vibrational actions. **e**, Absorption spectra of

the cyanine molecules and assignment of the vibrational collective oscillation (vibronic mode), LMP and TMP. The emission spectrum of the LED source is shown overlapped on the absorption spectra of the cyanine molecules. The emission spectrum of the LED shows $\lambda_{\text{max}} = 734 \text{ nm}$ and full-width at half-maximum = 35 nm. The LED light excites mostly the vibrational mode in Cy7.5-amine but not in Cy7-amine. Emission spectrum data for the LED from Prizmatix. **f**, General proposed working mechanism of MJH opening of cell membranes.

the rotational frequency of molecular motors to higher wavelengths, one that can rotate in the NIR frequency has yet to be reported^{2,3,8}. In this study, we leveraged a type of molecular mechanical action on cells induced by single-photon NIR light. We discovered that when we activate the vibronic mode of a cell-membrane-associated molecule, it results in concerted whole-molecule vibration^{9–11}, on subpicosecond timescales¹², inducing rapid cell death. Cell-associated molecular jackhammers (MJHs) exhibiting this concerted whole-molecule vibronic-driven action (VDA) have a mechanical action distinct from the UV-visible-activated unidirectional rotary molecular drills based on the Feringa and Dube designs^{2,4,13}.

In a typical molecular absorbance of photons, an individual bond or small portion of the molecule vibrates (Fig. 1a) or many bonds vibrate in a disconcerted manner (Fig. 1b). However, there is another way to

excite a molecule, wherein a whole-molecule vibration, or collective vibration, is achieved that is of a much longer-range and concerted, spreading through the entire length or width of the molecule (Fig. 1c). When vibrational and electronic modes, sometimes called phonon and plasmon modes, respectively, are coupled, the two modes together result in vibronic coupling^{11,14}, or it can be called molecular plasmon–phonon coupling¹⁰. After the initial excitation of a molecular plasmon in a suitable molecular structure, the collective electron oscillation decays rapidly in the femtosecond timescale due to interactions of the electrons with the atomic nuclei. This results in the electron–phonon damping process that induces a simultaneous collective oscillation of the nuclei, a collective vibration, typically in the subpicosecond timescale^{12,15–18}. This occurs via non-radiative decay during the internal conversion process with vibrational relaxation (see the Jablonski

diagram in Supplementary Fig. 1)¹². In summary, through the absorbance of a suitable energy of light, a molecule's collective electronic excitations hybridize with the molecule's vibrational modes to induce the vibronic mode¹¹. The vibronic mode is analogous to an ultrafast breathing mode of a molecule, where the entire molecule vibrates in unison throughout its length and its width because both longitudinal or transverse collective vibration, respectively, may occur^{10–12}. The existence of these longitudinal and transverse collective vibrations in molecules, also referred to as molecular plasmons as they are coupled processes, were first described theoretically by Cui et al. in 2016 and more recently observed experimentally by Kong et al. in 2021^{10,11}.

Here we show that when a suitable vibronic-mode-supported molecule is bound to a cell membrane, it can rapidly compromise the integrity of the membrane in a manner and rate that no partial molecular vibration (Fig. 1a) or disconcerted vibrations (Fig. 1b) can induce. Heating a molecule through photothermal therapy can cause many vibrations in a molecule, but those vibrations are not coordinated (Fig. 1b), hence there is no concerted longitudinal or transverse vibration that is sufficient to rapidly open a cell membrane. High powers and extended times are therefore required in photothermal therapy to cause slower apoptotic death. Conversely, VDA of a cell-associated molecule results in rapid necrosis even at very low energies. While photodynamic therapy generates ROS, VDA from a cell-associated molecule causes cell death that is unaffected by large doses of ROS inhibitors. Cyanine dyes have been used in photothermal and photodynamic therapies and they are readily accepted in biological and medicinal studies^{19–23}. We have exploited the VDA of these classical structures to kill cells 10–50 times faster than can be achieved with photothermal or photodynamic therapies, with concentrations 10 times lower than are generally used and with 10–50 times lower power than is often used (80 mW cm⁻² instead of 1–4 W cm⁻²).

Results and discussion

Vibrational excitation of aminocyanines

Cyanine structures are characterized by an odd-numbered polyene linker connecting two nitrogen-containing heterocycles with unusual photophysical properties^{24–28}. The absorption spectra of cyanines are dominated by an absorption band in the visible–NIR electromagnetic spectrum with a shoulder located at higher energy (shorter wavelength). Cy7.5-amine has an additional aryl ring in each of the heterocyclic moieties compared with Cy7-amine (Fig. 1d), which increases the conjugation, causing a redshift of its absorption by ~40 nm relative to Cy7-amine.

We postulated that the higher-energy shoulder next to the large absorption band in symmetrical cyanine structures results from the coupling of a molecular plasmon (a dominant collective oscillation of electronic excitation) to a dominant collective vibrational excitation, in agreement with the suggestion in the literature that the absorption sub-bands in the spectra of cyanines are primarily determined by a dominant symmetric vibration rather than a collection of single vibrations⁹. This vibronic behaviour, through the coupling of electronic and vibrational states, is a feature of conjugated-backbone near-symmetrical cyanines, such as Cy7-amine and Cy7.5-amine. The shoulder ($\lambda \approx 730$ nm) in the absorption spectrum of Cy7.5-amine corresponds to this collective vibrational mode (Fig. 1e). The same collective vibrational mode is present in Cy7-amine, but at ~690 nm. The molecular plasmons in cyanines were indeed confirmed by time-dependent density functional theory (TD-DFT) calculations; these molecules can support longitudinal molecular plasmons (LMPs) and transversal molecular plasmons (T MPs; Fig. 1d,e and Extended Data Fig. 1). The shoulder band (730 nm by experiment, 750 nm by TD-DFT calculation) is not the only vibronic mode present in the absorption spectrum of Cy7.5-amine, but rather the strongest in vibronic character spreading throughout the length and width of the molecule (Supplementary Video 1 and Supplementary Fig. 2). This can be observed by contrasting

the vibrational mode of the 750 nm shoulder in Supplementary Video 1 with the other concerted vibrational modes at 809, 530 and 430 nm in Supplementary Videos 2–4, respectively, obtained from first-principles TD-DFT vibrational calculations. The larger band at ~780 nm (809 nm calculated by TD-DFT), predominantly a longitudinal charge density resonance, the small peak at ~400 nm (430 nm calculated by TD-DFT), primarily a transversal charge density resonance, and the shoulder at ~450 nm (530 nm calculated by TD-DFT), with a predominant short longitudinal charge density resonance, also have vibronic properties with charge density resonances typical of a molecular plasmon¹⁰ (Extended Data Fig. 1). It is important to recognize that the TD-DFT calculations describe more accurately the longer wavelengths (780 and 730 nm) of the absorption bands in the spectrum. The longitudinal contributions to the resonances at the shorter wavelengths (~400–600 nm) are inaccurately overestimated by TD-DFT (Extended Data Fig. 1a–c).

Previously, Yang et al. resolved a vibrational frequency at 1,310 cm⁻¹ (this is equivalent to 25 fs per oscillation or a frequency of 4×10^{13} s⁻¹) for 1,1',3,3,3',3'-hexamethyl-4,4',5,5'-dibenzo-2,2'-indotricarbocyanine using wavelength-resolved femtosecond pump–probe spectroscopy when the vibronic shoulder was selectively excited; however, the identity of the absorption shoulder was not explained in that study¹⁸. Given that our TD-DFT analysis strongly supports that the absorption shoulder represents the concerted whole-molecule vibronic mode, we can expect that this reported band at 1,310 cm⁻¹ corresponds to the vibrational frequency of the concerted whole-molecule vibration. Corroborating this assumption, this frequency has been reported to correspond to one dominant vibration with a nearly constant value (~1,310–1,375 cm⁻¹) in indocyanine structures. This value matches the energy spacing between the two dominant absorption sub-bands, which represent the vibronic shoulder next to the absorption peak^{9,28}. Moreover, resonance Raman spectroscopy has determined that this is an intensity-dominant vibrational band at 1,365 cm⁻¹ in the spectrum of Cy5 and confirmed for other cyanines^{29,30}. Specifically, for Cy7.5 this vibrational frequency has been measured at ~1,370 cm⁻¹ (this is 24 fs per oscillation or a frequency of 4.1×10^{13} s⁻¹) using Raman spectroscopy³⁰. These subpicosecond concerted whole-molecule vibrations are terahertz-timescale (41 THz) oscillations, that is, they are seven orders of magnitude faster than the megahertz (2–3 MHz) rotations elicited by Feringa-type motors¹.

MJH-mediated VDA on cells

We selectively excited the vibronic mode in a cell-membrane-bound Cy7.5-amine using a NIR light-emitting diode (LED) at 730 nm (Fig. 1e), which resulted in the permeabilization of the cellular membrane to 4',6-diamidino-2-phenylindole (DAPI; Fig. 1f). DAPI is a cell-membrane-impermeable dye in viable cells that mainly stains cellular DNA in membrane-disrupted cells. While 730 nm light does not excite the vibronic shoulder of Cy7-amine, it can activate Cy7.5-amine (Fig. 1e) and permeabilize A375 human melanoma cells immediately after treatment (Fig. 2a–f). It took ~30 s from the time the sample was irradiated to start collecting the data in the flow cytometer. For this experiment, 1 μM Cy7.5-amine and 730 nm LED irradiation at 80 mW cm⁻² for 10 min caused permeabilization to DAPI staining of 99.6% of the A375 cells in a cell suspension containing 2×10^5 cells. In contrast, Cy7-amine was not able to permeabilize the cells under the same conditions. This difference between the two aminocyanines supports the notion that the 730 nm light can excite the vibronic mode (shoulder) in Cy7.5-amine (Fig. 1e) causing cellular membrane permeabilization and ultimately cell death by necrosis, as seen by immediate DAPI staining. The flow cytometry measurements showed that both aminocyanines were attached efficiently to the cells in the absence of irradiation (Fig. 2b,c). It is interesting that Cy7-amine has a higher extinction coefficient ($\epsilon = 132,000$ M⁻¹ cm⁻¹) at $\lambda = 730$ nm than Cy7.5-amine ($\epsilon = 72,000$ M⁻¹ cm⁻¹) in water, yet Cy7-amine does not permeabilize the cells at comparable concentrations, while Cy7.5-amine

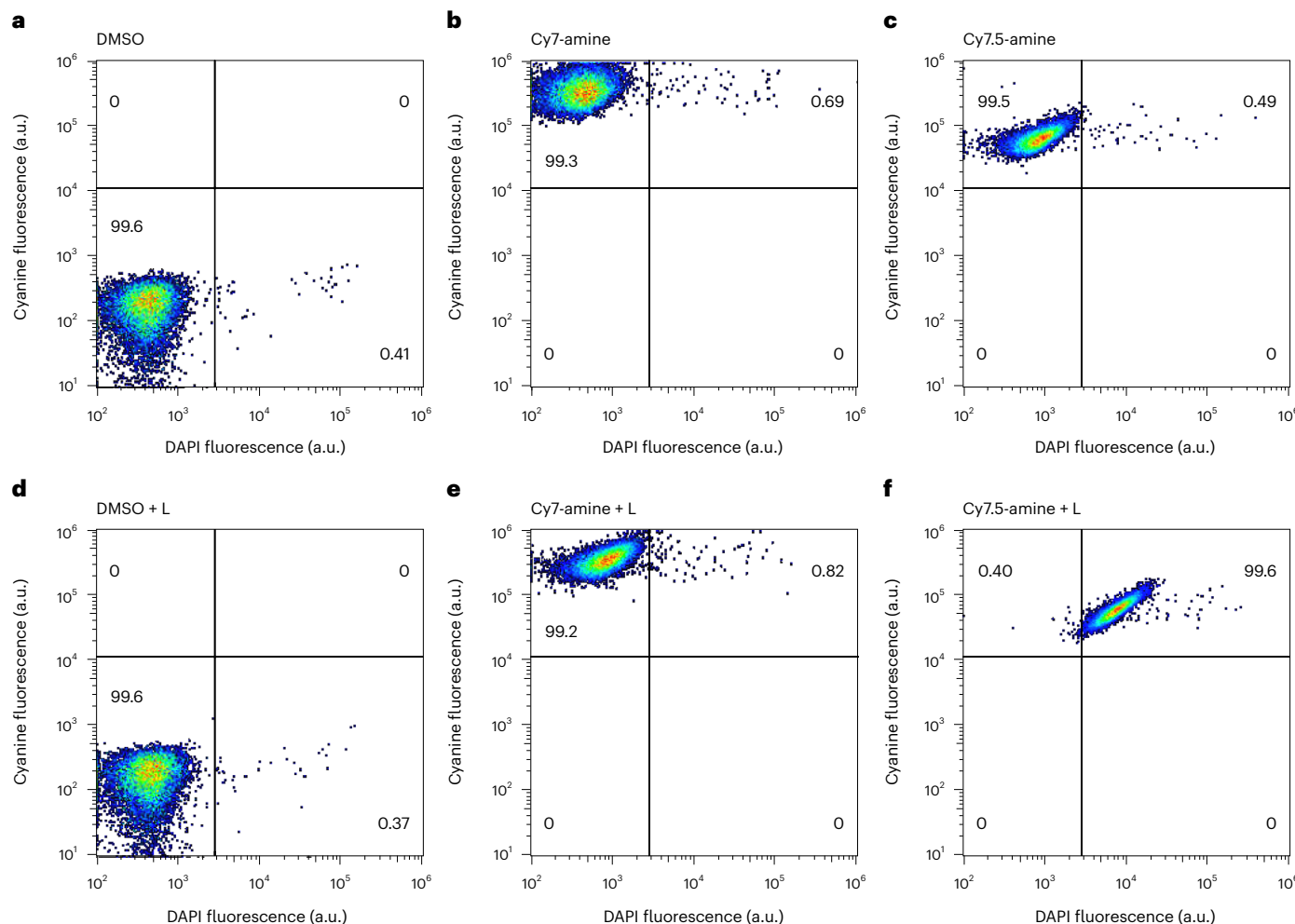


Fig. 2 | Flow cytometry analysis of MJH permeabilizing cell membranes. **a–f**, Fast A375 melanoma cell permeabilization to DAPI (DAPI enters and stains the membrane-disrupted cells, but more slowly with viable cells) immediately after treatment with 1 μM Cy7.5-amine or Cy7-amine excited with 730 nm NIR light (80 mW cm⁻² for 10 min) and analysed within ~1 min of light treatment: control 0.1% DMSO (**a**), Cy7-amine (**b**), Cy7.5-amine (**c**), control 0.1% DMSO + NIR light (L) treatment (**d**), Cy7-amine + NIR light treatment (**e**) and Cy7.5-amine + NIR light treatment (**f**). The numbers inside the gates (the four quadrants) in the flow

cytometry plots represent the percentage of cells in each gate: cyanine negative and DAPI negative (bottom left), cyanine positive and DAPI negative (top left), cyanine negative and DAPI positive (bottom right) and cyanine positive and DAPI positive (top right). All the cell suspensions for this study contained 0.1% DMSO; DMSO was used to presolubilize the cyanine molecules in 8 mM stock solutions in 100% DMSO. In this study, 10,000 cells were analysed for each condition. The flow cytometry data processing is described in detail in Supplementary Fig. 5.

permeabilizes the cells readily upon excitation (Fig. 2). This result suggests that a photothermal effect is not operating as Cy7-amine has a higher absorption cross-section than Cy7.5-amine at 730 nm. Likewise, photodynamic therapy is unlikely as the Cy7 and Cy7.5 cyanines have similar yields for singlet oxygen generation³¹. This will be discussed further below.

Structural elements in MJH and mechanism of action

A summary of the proposed working mechanism is described in Fig. 1f and expanded in Extended Data Fig. 2. The binding of the aminocyanine to the cells is possibly mediated through the interaction of the charge on its pendant amine moiety with the negatively charged phospholipids (Extended Data Fig. 3), and light-activated VDA opens the cell membranes. The structures of the MJHs and their classification according to their expected relative strength in the VDA (plasmonicity), based on the extension of the indole with polycyclic aromatic hydrocarbons and the length of the π-conjugation in the polymethine bridge, are presented in Extended Data Fig. 2. In another experiment, the amino-cyanine Cy5-amine was added as a competitor for cell binding against Cy7.5-amine; the results showed a reduction of the permeabilization

activity of Cy7.5-amine (Supplementary Fig. 3). The optical spectra of all of the aminocyanines used in this study and the characterization of their binding to A375 human melanoma cells by confocal microscopy are presented in Extended Data Fig. 4.

Consistent with the VDA proposed here, excitation of the 680 nm vibronic shoulder in Cy7-amine improves the MJH effect for opening cell membranes in A375 cells (Extended Data Fig. 5). However, the permeabilization is not as great as for 730 nm excitation of Cy7.5-amine, even when exciting the 680 nm shoulder of Cy7-amine using an equal light dose of 80 mW cm⁻² for 10 min. This might result because Cy7-amine lacks the extended aryl rings of Cy7.5-amine, limiting the TMP of the vibronic mode. Hence, Cy7-amine is a weaker MJH than Cy7.5-amine because of the lower plasmonicity of indole compared with benzoindole (Fig. 1d).

Structure–activity relationship in MJH-mediated cell membrane opening

We compared Cy7-amine and Cy7.5-amine by exciting various concentrations of these cyanines at 730 nm (Fig. 3), and observed that Cy7.5-amine is much more efficient at permeabilizing cells upon VDA

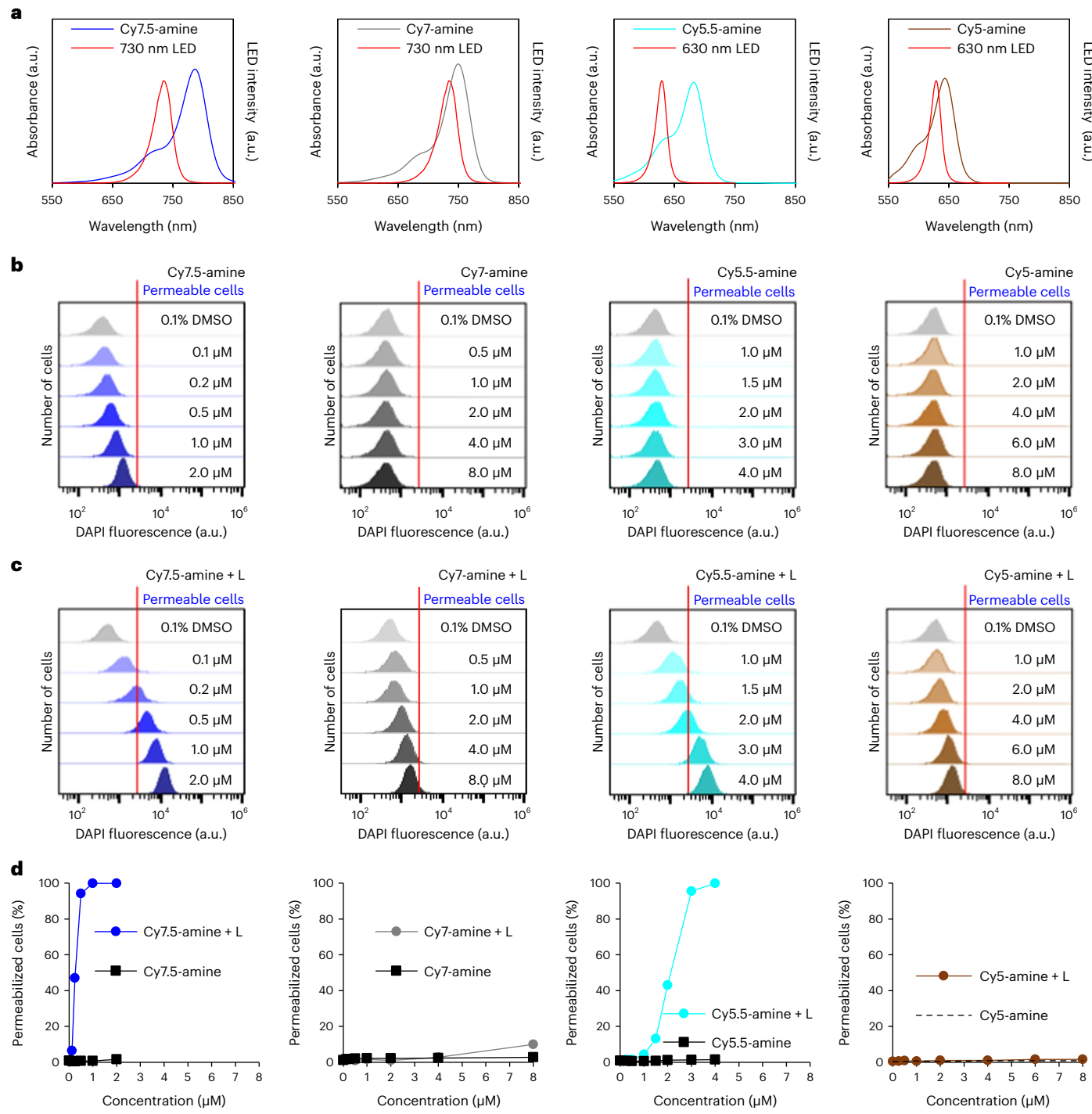


Fig. 3 | Dependence of cell membrane permeabilization on the expected strength of the MJHs. **a**, Absorption spectra of Cy7.5-amine, Cy7-amine, Cy5.5-amine and Cy5-amine overlaid with the spectrum of the specific LED light used for the illumination of each MJH. **b,c**, Flow cytometry analysis to measure the permeabilization of A375 cells in the presence of increasing concentrations of each MJH without illumination (**b**) and with specific LED illumination for each cyanine (**c**). The red line represents the gating to discriminate between DAPI negative and positive cells (permeable). **d**, Plots of the percentage of permeabilized cells versus the concentration of aminocyanine. The numbers of permeabilized cells were extracted from flow cytometry analysis. In this study, 10,000 cells were analysed at each concentration. The cells were incubated

with the MJHs for 30 min. The light-treated samples were illuminated with the same light dose of 80 mW cm^{-2} for 10 min. The shift of the DAPI fluorescence intensity for Cy7.5-amine before illumination corresponds to the fluorescence emission from Cy7.5-amine, which is excited with the same laser that excites DAPI ($\lambda_{\text{ex}} = 405 \text{ nm}$). This conclusion is supported by the confocal microscopy data in Extended Data Fig. 3. The level of fluorescence from Cy7.5-amine can be regarded as background fluorescence and not cell membrane permeabilization. This was the main factor that was considered when drawing the position of the gating (red line) to discriminate between DAPI positive and negative cells. The flow cytometry data processing is described in detail in Supplementary Fig. 5.

induced by NIR light. Even at much higher concentrations of Cy7-amine (8 μM), it does not permeabilize cells as efficiently as lower concentrations of Cy7.5-amine. These results further support that the excitation

of the vibronic shoulder in Cy7.5-amine at 730 nm and the extension of the conjugation by the aryl rings in the benzoindoles are critical to maximize the VDA. Another aminocyanine family, Cy5.5-amine and

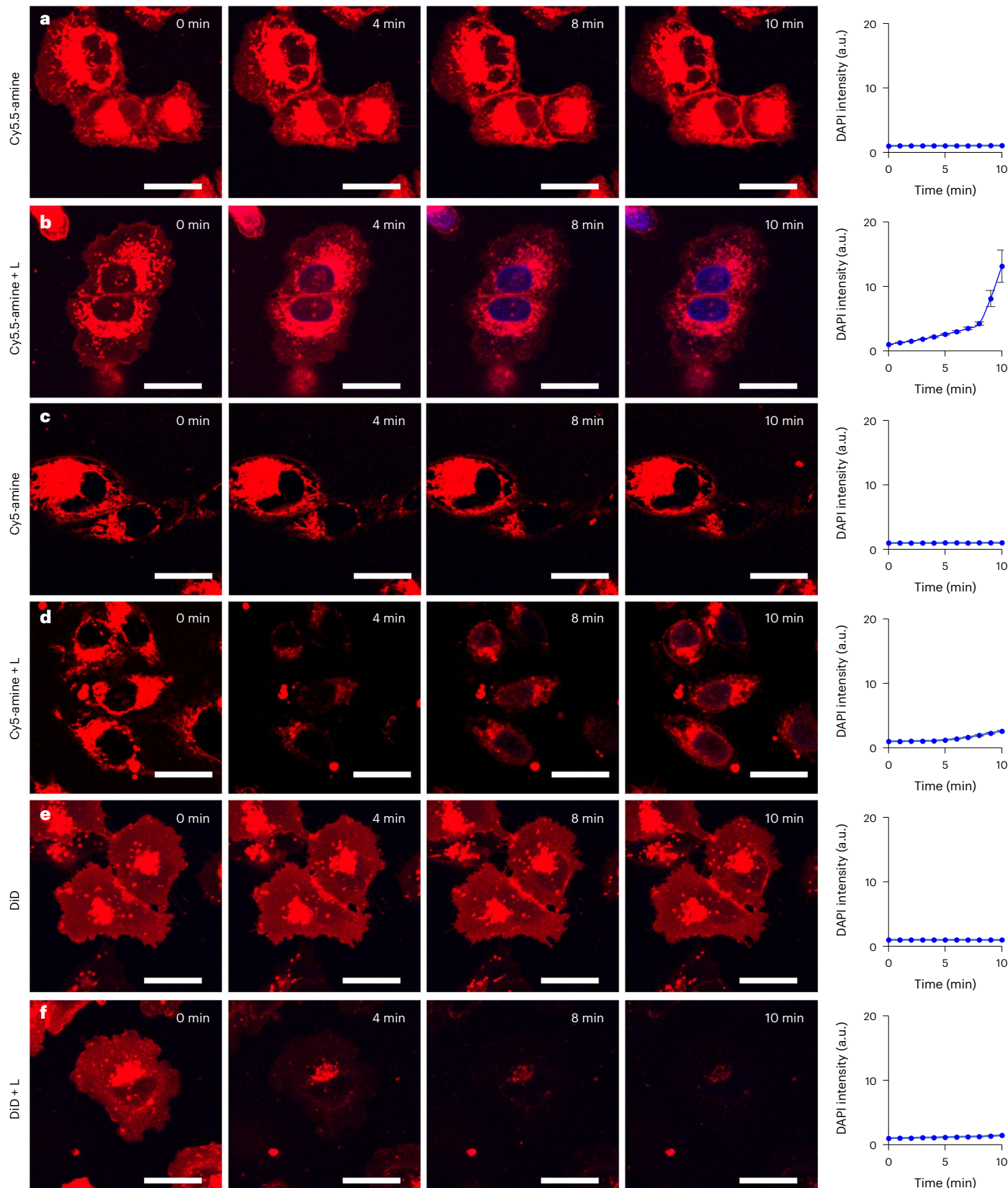


Fig. 4 | Cell membrane permeabilization of A375 cells over time. Confocal spectroscopy images of the permeabilization of DAPI into A375 cells upon irradiation as a function of time (left) and the corresponding plots of DAPI intensity versus time (right). **a,b**, Cells in the presence of 4 μ M Cy5.5-amine without laser irradiation (**a**) and with 640 nm laser irradiation (**b**). **c,d**, Cells in the presence of 4 μ M Cy5-amine without laser irradiation (**c**) and with 640 nm laser irradiation (**d**). **e,f**, Cells in the presence of cell-membrane-targeting 4 μ M DiD dye without laser irradiation (**e**) and with 640 nm laser irradiation (**f**).

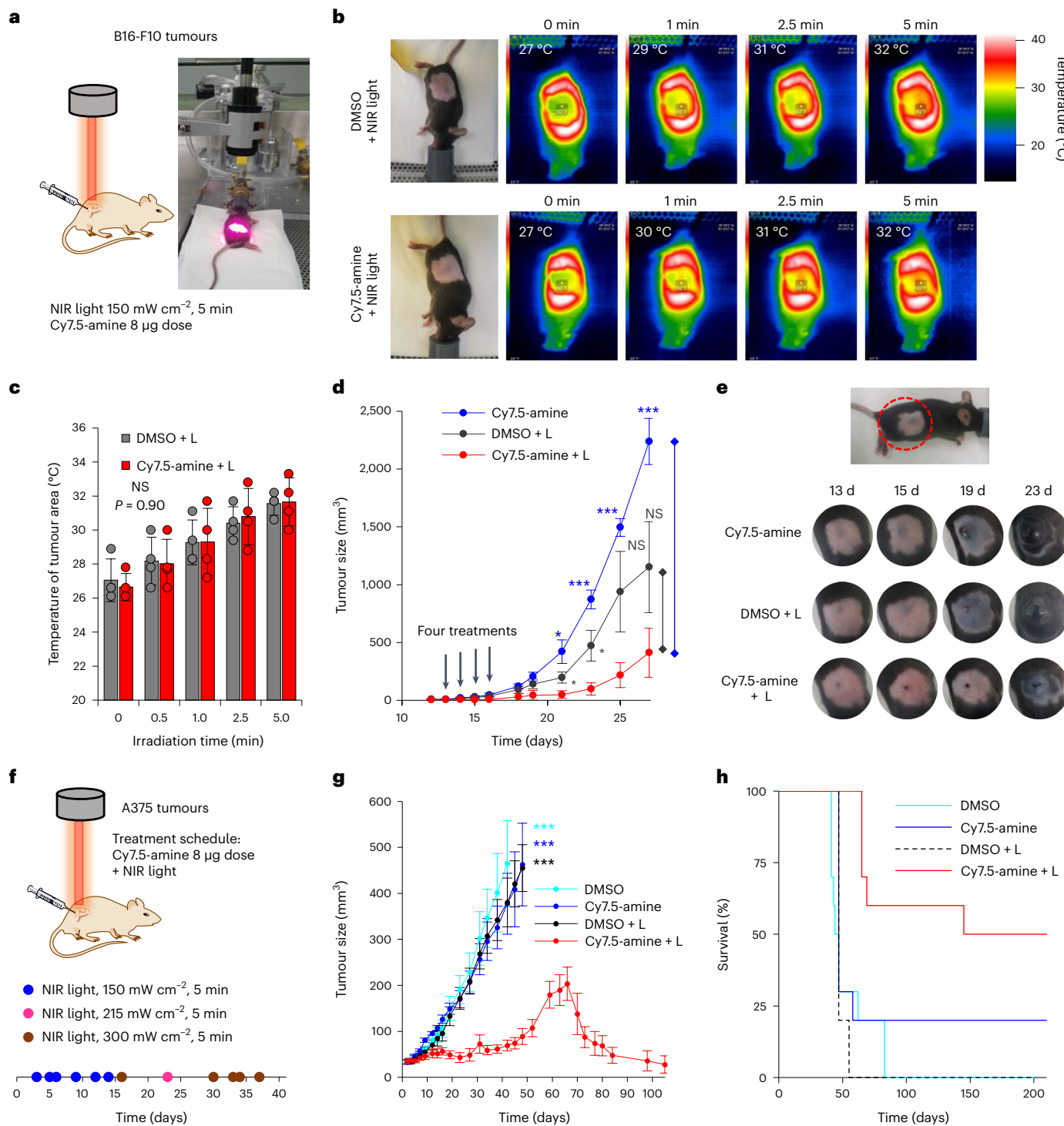
The irradiation times are shown in each image. To activate the MJH effect, the cells were irradiated at $\lambda_{\text{ex}} = 640$ nm at 25% (250 μ W) power. Images were recorded every 1 min at low photoactivation powers and short exposures ($\lambda_{\text{ex}} = 640$ nm, 5% (5 μ W) power, 2.1 s per frame) to maintain as intact as possible the non-irradiated controls. The cells were incubated with the cyanines for 30 min before irradiation. Representative confocal images of each condition are shown. The plots on the right show averaged data of 14 cells ($n = 14$); the error bars represent standard errors. Scale bars, 25 μ m.

the GUVs upon photoactivation using 640 nm laser excitation to actuate the vibronic mode. The mechanistic steps involved are presumed to be as follows: (1) the MJH Cy5.5-amine binds to the lipid bilayers, (2) the photoactivated VDA disassembles the phospholipid domains in close contact with the MJH, generating vacancies or holes, (3) the remaining phospholipids in the bilayers reorganize by hydrophobic interaction through the tails to fill the vacancies and the GUVs shrink in size (Extended Data Fig. 10b, at 20 s), and (4) the photoactivated VDA continuously generates holes until at some point the GUVs burst (at ~30 s). Here we observed the shrinking of the GUVs, in contrast to the photodynamic therapy effects of ROS, where the expansion of the lipid bilayers in GUVs is observed^{34,35}. The Cy5-amine control, a weaker MJH,

does not exert enough VDA when used at 2 μM to disassemble the GUVs (Extended Data Fig. 10d). This is consistent with the results obtained with A375 cells (Figs. 3 and 4). These results with GUVs suggest that MJHs disrupt lipid bilayers through mechanical action generated by VDA.

MJH-mediated anti-tumour activity *in vivo*

The MJH Cy7.5-amine was applied to treat murine (B16-F10) and human (A375) melanoma tumours in mice (Fig. 5a). The temperature of the B16-F10 tumours in C57BL/6 mice treated with Cy7.5-amine and 730 nm light (150 mW cm^{-2} for 5 min) increased ~5 °C, which is the same increase as observed in the control with 0.1% dimethylsulfoxide (DMSO) and light (Fig. 5b,c). The size of the B16-F10 tumours was substantially reduced



29. Yang, J.-P. & Callender, R. H. The resonance Raman spectra of some cyanine dyes. *J. Raman Spectrosc.* **16**, 319–321 (1985).
30. Yu, J. H. et al. Noninvasive and highly multiplexed five-color tumor imaging of multicore near-infrared resonant surface-enhanced Raman nanoparticles *in vivo*. *ACS Nano* **15**, 19956–19969 (2021).
31. Štacková, L. et al. Deciphering the structure–property relations in substituted heptamethine cyanines. *J. Org. Chem.* **85**, 9776–9790 (2020).
32. Zhao, J., Wu, W., Sun, J. & Guo, S. Triplet photosensitizers: from molecular design to applications. *Chem. Soc. Rev.* **42**, 5323–5351 (2013).
33. Itri, R., Junqueira, H. C., Mertins, O. & Baptista, M. S. Membrane changes under oxidative stress: the impact of oxidized lipids. *Biophys. Rev.* **6**, 47–61 (2014).
34. Riske, K. A. et al. Giant vesicles under oxidative stress induced by a membrane-anchored photosensitizer. *Biophys. J.* **97**, 1362–1370 (2009).
35. Sakaya, A. et al. Singlet oxygen flux, associated lipid photooxidation, and membrane expansion dynamics visualized on giant unilamellar vesicles. *Langmuir* **39**, 442–452 (2023).
36. Zonios, G., Bykowski, J. & Kollias, N. Skin melanin, hemoglobin, and light scattering properties can be quantitatively assessed *in vivo* using diffuse reflectance spectroscopy. *J. Invest. Dermatol.* **117**, 1452–1457 (2001).
37. Haussmann, P. B. et al. Melanin photosensitization by green light reduces melanoma tumor size. *J. Photochem. Photobiol.* **9**, 100092 (2022).
38. Liu, D., Huang, H., Zhao, B. & Guo, W. Natural melanin-based nanoparticles with combined chemo/photothermal/photodynamic effect induce immunogenic cell death (ICD) on tumor. *Front. Bioeng. Biotechnol.* **9**, 635858 (2021).

Publisher's note Springer Nature remains neutral with regard to jurisdictional claims in published maps and institutional affiliations.

Springer Nature or its licensor (e.g. a society or other partner) holds exclusive rights to this article under a publishing agreement with the author(s) or other rightsholder(s); author self-archiving of the accepted manuscript version of this article is solely governed by the terms of such publishing agreement and applicable law.

© The Author(s), under exclusive licence to Springer Nature Limited 2023

groups (four samples per group): (1) 0.1% DMSO, (2) 0.1% DMSO + NIR light treatment, (3) 2 μ M Cy7.5-amine and (4) 2 μ M Cy7.5-amine + NIR light. The treatments with 0.1% DMSO or 2 μ M Cy7.5-amine were conducted by adding those respective concentrations to the cells in the media, followed by incubation for 60 min. Immediately after incubation, the cells in the groups with '+ NIR light' were treated with 730 nm light at 80 mW cm⁻² for 10 min. After the treatment with NIR light, the media was removed from the cell suspensions of all groups and fresh media was added. Then, the cells were incubated for 2 days at 37 °C and 5% CO₂. At the end of the incubation, the media was removed and the cells washed once with 500 μ l PBS. The cells were stained with 500 μ l of 0.5% (w/v) crystal violet solution in methanol–water (1:1) for 5 min. Excess crystal violet was removed by washing with water. The cells contained in the 24-well plate were dried at room temperature. Then, the crystal violet in each well was solubilized in 500 μ l of 3.3% (v/v) acetic acid in water and the total crystal violet recovered in this acidic solution. Finally, the crystal violet was quantified by its absorbance at 570 nm. The cell viability was calculated from the absorbance relative to the absorbance of crystal violet from cells without any treatment; the cells without treatment were normalized to 100% cell viability.

Clonogenic assay

A375 cells were seeded in 35-mm cell culture dishes at predetermined densities to allow for an approximately equal number of resultant colonies. The next day, the cells were treated with Cy7.5-amine at variable concentrations with and without 730 nm light illumination at 80 mW cm⁻² for 10 min. The cells were incubated with Cy7.5-amine for 50 min before illumination, while the media was replaced with fresh media after illumination and the cells cultured for 6 days to allow for colony formation. The cells were then washed once with PBS and fixed-stained in 0.5% (w/v) crystal violet in methanol–water (1:1) during 10 min. Excess crystal violet was washed off with water, the plates were dried at room temperature, and then the colonies were counted using ImageJ software (version 1.52a) and the survival fraction was determined. All treatments were performed in triplicate.

ROS measurements using 2',7'-dichlorodihydrofluorescein diacetate

2',7'-Dichlorodihydrofluorescein diacetate (H₂DCF-DA) is a cell permeant reagent. It is deacetylated by cellular esterases to form H₂DCF, a non-fluorescent compound that is rapidly oxidized in the presence of ROS to 2',7'-dichlorofluorescein (DCF). DCF is highly fluorescent and its excitation and emission are detected at 488 and 535 nm, respectively. A suspension of A375 cells containing 2 \times 10⁵ cells ml⁻¹ was first prepared in DMEM media without phenol red. Then, the cells were incubated for 30 min at 37 °C with Cy7.5-amine (or the other cyanines), typically at a concentration of 2 μ M in the media. Next, H₂DCF-DA (Sigma-Aldrich) was added to the cell suspension in media to a final concentration of 5 μ M (the concentration of the H₂DCF-DA stock solution was 5 mM in DMSO stored at -20 °C). The cells were then transferred to a 96-well plate, 100 μ l in each well. Typically, it took 15 min to transfer all the samples and all the controls into the 96-well plate, 6 repetitions for each treatment condition: cyanine + light, cyanine only, DMSO + light, DMSO only, cells only and media only. Immediately after the transfer, the cells were treated with NIR 730 nm light at 80 mW cm⁻² for 10 min. From the time the H₂DCF-DA was added to the cell suspension to the time the cells were treated, there was in total a 20 min period of incubation. The DCF fluorescence intensity was measured immediately after the light treatment using a 96-well plate reader at $\lambda_{\text{ex}} = 488/9$ nm and $\lambda_{\text{em}} = 535/20$ nm. The measurements were normalized with respect to the fluorescence intensity of the media only.

Singlet oxygen measurements

Singlet oxygen was measured using the molecular probe 1,3-diphenylisobenzofuran (DPBF), which decomposes in the presence

of singlet oxygen, and this was detected by the change in the absorbance of DPBF at 410 nm. DPBF was freshly prepared for every experiment by dissolving DPBF in methanol to yield a 1 mM stock solution. This DPBF solution was diluted in methanol, with the dilution volume adjusted to achieve an absorbance of ~1.0 at 410 nm. For this purpose, typically 170 μ l of the 1 mM DPBF stock solution in methanol was diluted in 2,830 μ l methanol. Then, to this mixture was added 1 μ l cyanine stock solution (8 mM cyanine solution in DMSO stored at -20 °C) to yield a final concentration of 2.6 μ M cyanine. Immediately after preparing this mixture, the solution was transferred to a clean spectrophotometer quartz cuvette, and the solution was irradiated with 730 nm LED light at a power intensity of 80 mW cm⁻². The power intensity was calibrated to the distance at the top of the liquid in the quartz cuvette. The sample was irradiated intermittently in periods of 30 s and the absorption spectrum was recorded in between every irradiation step until a total irradiation time of 10 min had accumulated; there were 20 periods of irradiation of 30 s each.

Synthesis of DPhPC GUVs

GUVs were synthesized using the gel-assisted formation method with some minor modifications³⁹. Briefly, the fully saturated phospholipid DPhPC (Avanti Polar Lipids, 850356) was dissolved in anhydrous chloroform at 1 mg ml⁻¹ and stored at -20 °C. A microscopy cover glass was flamed for ~5 s in a Bunsen burner. Then, 250 μ l of 5% (w/v) poly(vinyl alcohol) (PVA) in deionized water was spread over the surface of the cover glass and dried overnight at 50 °C. Next, 30 μ l of the 1 mg ml⁻¹ DPhPC solution in chloroform was spread over the surface of the PVA-coated cover glass and dried at room temperature overnight. Subsequently, ~250 μ l PBS buffer (Corning, 21040CV) was added onto the cover glass to allow the hydration and formation of GUVs over a period of 1–2 h. Then, the GUVs were collected by pipetting up and down to help to detach the GUVs from the surface and then transferred to an Eppendorf tube and stored at 4 °C.

In vivo studies

All of the animal studies were approved (protocol number 00000950-RN03) by the Institutional Animal Care and Use Committee (IACUC) of the University of Texas MD Anderson Cancer Center. In our studies, we used 7–8-week-old female C57BL/6J mice (Jackson Laboratories, strain 000664) or 7–8-week-old athymic female nude (nu/nu) mice (Envigo). According to the approved IACUC protocol, the tumour size did not exceed 2 cm in any direction in the mice. The housing conditions of the mice were as follows: temperature 22 °C (high 23.5 °C, low 21 °C), humidity 45% (high 55%, low 40%) and 12 h light/dark cycle.

Generation of B16-F10 melanoma tumours in C57BL/6J mice

The B16-F10 cells were cultured as described above. The cells were collected from subconfluent plates (~90%), with fresh media added to the cells the day before collection. The cells were collected using 0.05% trypsin–EDTA (Gibco, 25-300-054) and then redispersed in DMEM media without supplements at 1 \times 10⁶ cells ml⁻¹. The cell suspension was kept in ice. Then, 100 μ l of cells was injected per mouse (100,000 cells per mouse) subcutaneously into the right flank of a 7–8-week-old female mouse (C57BL/6J), the hair on the right flank having been previously depilated using a shaver. The tumours were allowed to grow for 12 days, counting from the day of cell injection. At day 12, the hair of the mouse was removed using hair remover cream (Nair Hair Remover Lotion). For this purpose, a drop of the cream was applied to the skin over the area where the tumour cells were injected. The mice were anaesthetized using isoflurane while the hair remover cream was applied. Starting at day 12, the tumours were measured using a calliper. The tumours could be observed as a black spot (due to the melanin present in the B16-F10 cells) under the skin after the cream depilation. Typically, the volume of the tumours at ~15 days

C.A.-O. designed and conducted the *in vivo* experiments. A.C. injected the cancer cells to generate the tumours and assisted in monitoring the mice. R.R. and J.N.M. oversaw the *in vivo* experiments, provided the mice and established the B16-F10 tumour model. D.G.-A. and J.M.S. conducted the TD-DFT calculations of molecular plasmons in Cy7.5-amine. C.A.-O. and J.M.T. wrote the manuscript. All authors read and approved the manuscript.

Competing interests

Rice University owns the intellectual property on the use of MJH coupled with VDA for the permeabilization of cell membranes. C.A.-O. is a former subcontractor to Nanorobotics, the possible licensee of this technology from Rice University. J.M.T. is a stockholder in Nanorobotics, but not an officer, director or employee. Conflicts are mitigated through regular disclosure to and compliance with the Rice University Office of Sponsored Programs and Research Compliance. The remaining authors declare no competing interests.

Additional information

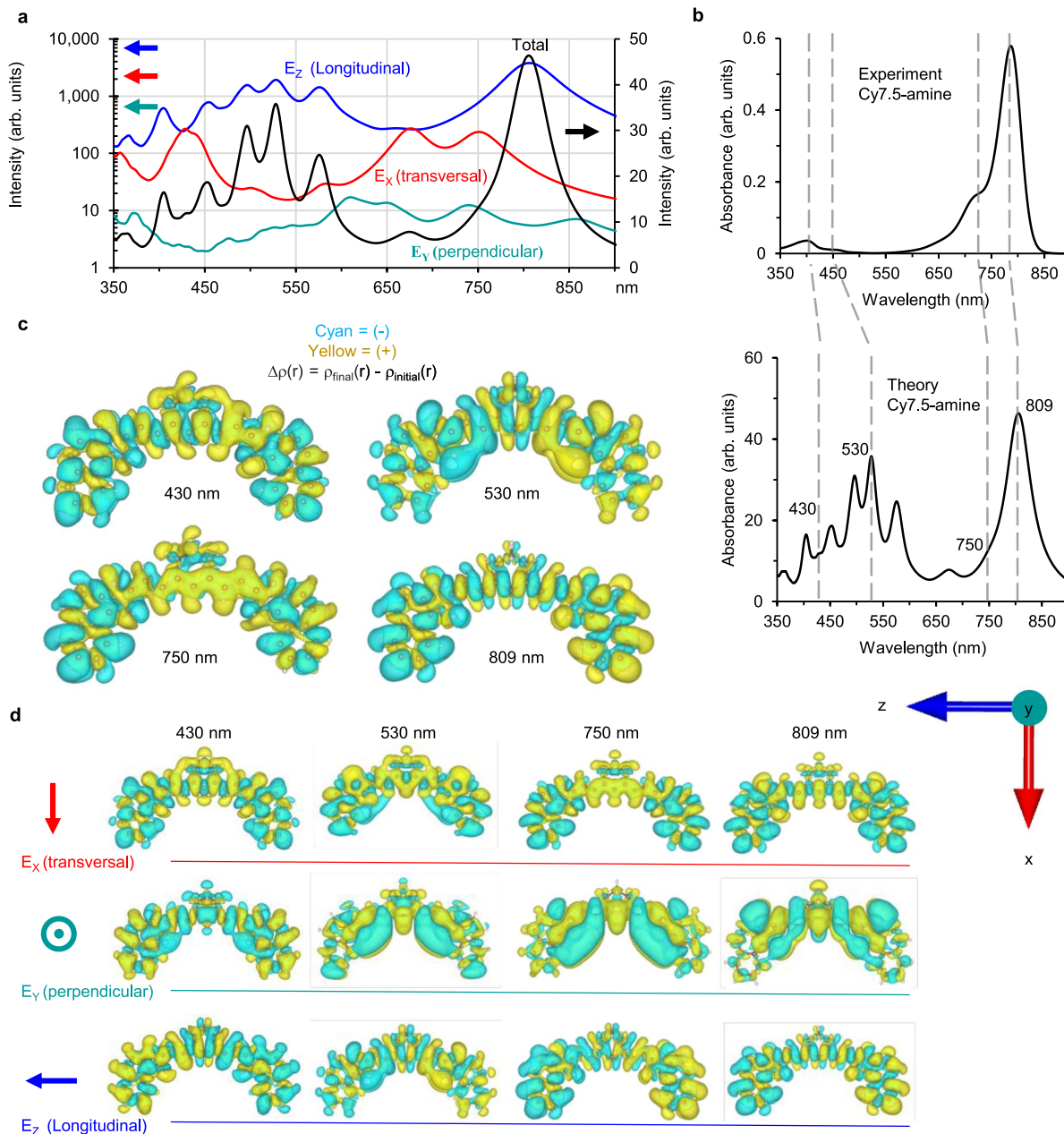
Extended data is available for this paper at
<https://doi.org/10.1038/s41557-023-01383-y>.

Supplementary information The online version contains supplementary material available at <https://doi.org/10.1038/s41557-023-01383-y>.

Correspondence and requests for materials should be addressed to Ciceron Ayala-Orozco, Jorge M. Seminario, Jeffrey N. Myers or James M. Tour.

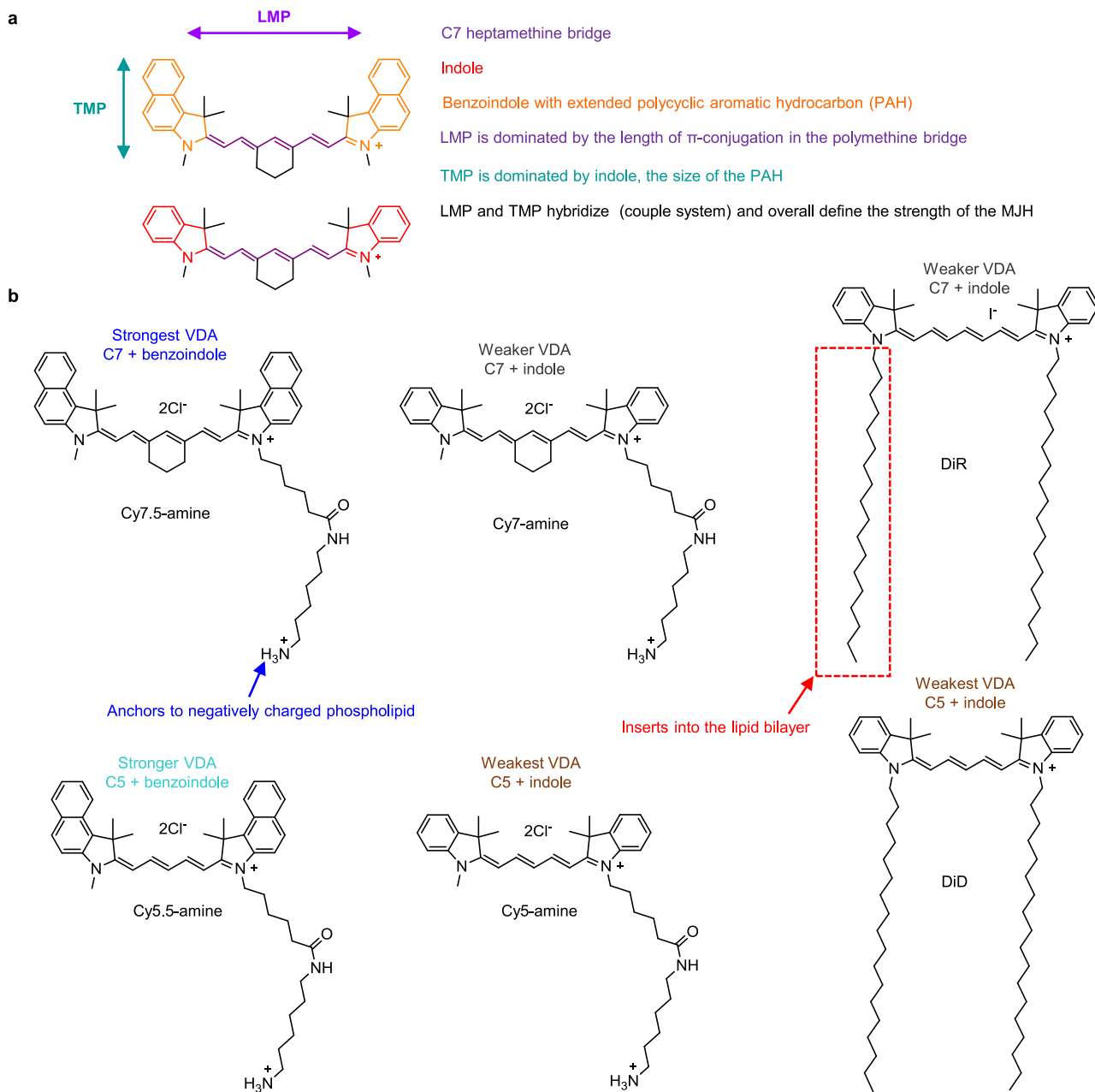
Peer review information *Nature Chemistry* thanks Weian Zhang and the other, anonymous, reviewer(s) for their contribution to the peer review of this work.

Reprints and permissions information is available at
www.nature.com/reprints.



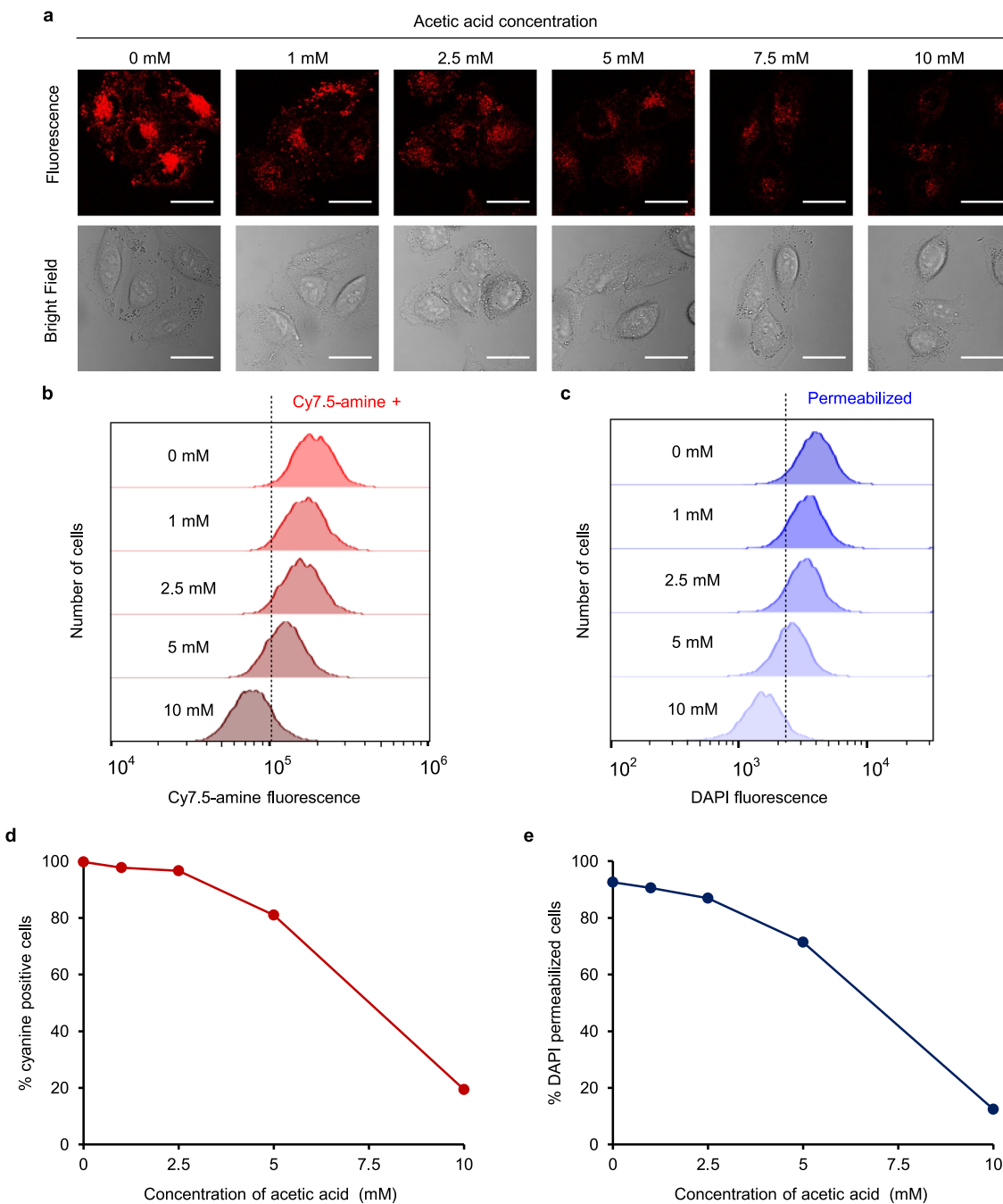
Extended Data Fig. 1 | Calculated TD-DFT absorption spectrum and induced charge density plots of the molecular plasmons in Cy7.5-amine. (a) Total and partial, by the orientation of the electric field component (E_i), absorption spectra calculated by time-dependent density-functional theory (TD-DFT) using the Lanczos approach. The electric field is used to simulate the optical excitation of the Cy7.5-amine. The partial components of the spectrum are oriented along the transversal molecular plasmon resonance (red), longitudinal (blue) and perpendicular (teal) axis of Cy7.5-amine. (b) Absorption spectra comparison between the experimental (top) and the TD-DFT calculation (bottom). The dashed lines represent the position of the wavelengths at which the induced charge density maps were calculated for molecular plasmon resonances. The experimental shoulder at 730 nm for the vibronic mode in Cy7.5-amine is

observed at 750 nm in the theoretical transversal component of the spectrum, but it is less obvious in the total spectrum. (c) Total induced charge densities [$\Delta\rho(r)$] at 430, 530, 750 and 809 nm wavelengths for molecular plasmon resonance. (d) Induced charge densities [$\Delta\rho(r)$] by electric field (E_i) components at 430, 530, 750 and 809 nm wavelengths oriented along the transversal, longitudinal and perpendicular axis of Cy7.5-amine. The vectors on the rightmost represent the orientation of the electric field components. The long alkyl-amine arm in Cy7.5-amine structure was not included in the electronic structure calculation because it has negligible contributions to the conjugation of the core structure. Instead, a methyl group was substituted for the long alkyl-amine in Cy7.5-amine.



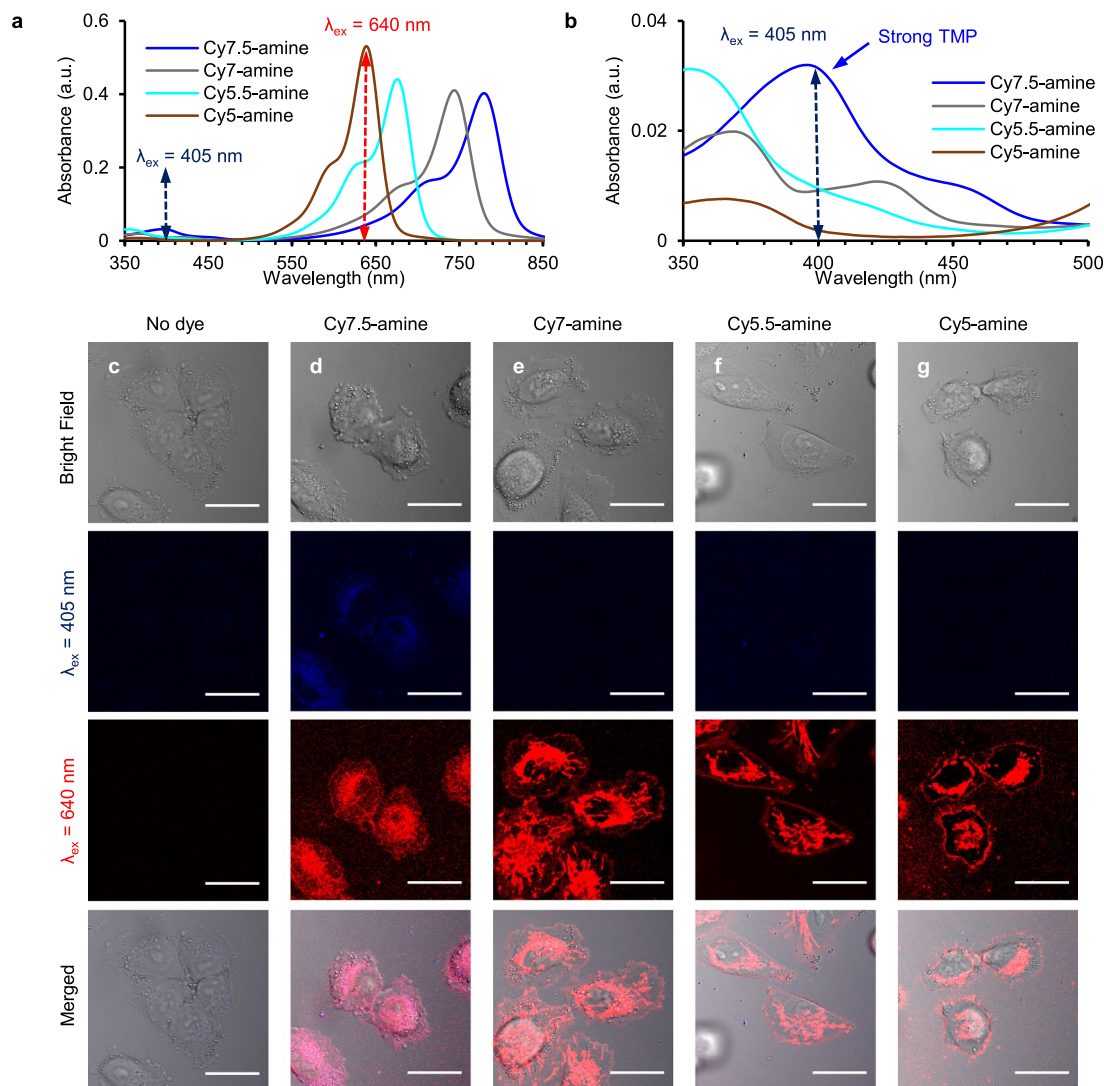
Extended Data Fig. 2 | Molecular jackhammer (MJH) model and summary of structures used in this study. (a) Important MJH structural elements. LMP = longitudinal molecular plasmon. TMP = transversal molecular plasmon. The strength of the molecular plasmon (VDA) is expected to be proportional to the length of the π -conjugation. The π -conjugation can be increased in two ways: 1) increasing the length of polymethine bridge and 2) increasing the size of the polycyclic aromatic hydrocarbon (PAH) fused to the indole. The purple color is to highlight the polymethine bridge. The cyanines are named by the number of carbons in the polymethine bridge, in the example it is C7. The red color is to highlight the structure of the indole, and the orange color is for the

benzoindole. The heptamethine bridge (C7) can be chemically conjugated with indole to form Cy7 or with benzoindole to form Cy7.5. These structural elements, polymethine and indole or benzoindole, hybridize to form a coupled system with the molecular plasmon-dominated longitudinally by the polymethine bridge (LMP in purple) and transversally by the indole or benzoindole (TMP in teal). However, these structures are hybridized and the electronic conjugation of the benzoindole influences the polymethine bridge and *vice versa*. (b) Summary of structures in this study. The observed effect on the cell killing is summarized for each structure, and each lists the common name of the conjugate backbone. The addend function is listed for each.



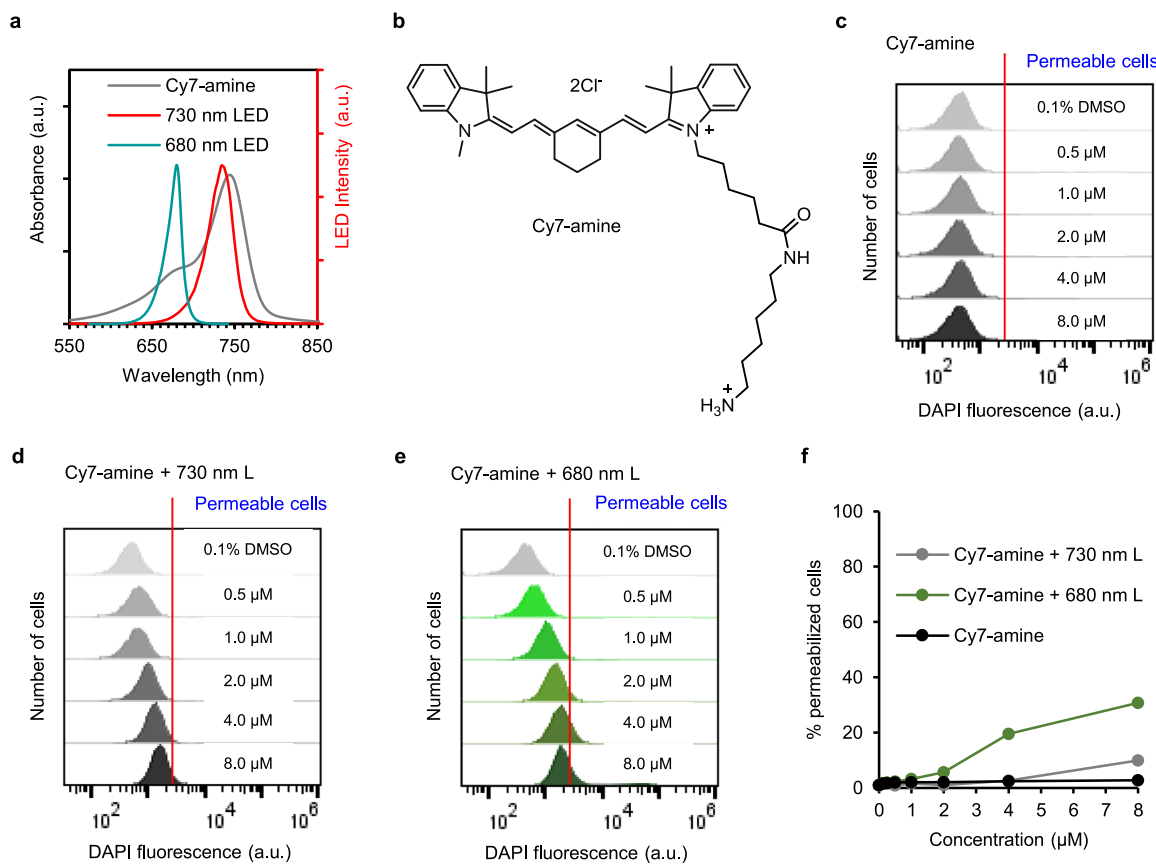
Extended Data Fig. 3 | Binding of MJH into the external cellular membrane and into internal organelle membranes of A375 human melanoma cell line. (a) Fluorescence confocal microscopy imaging of MJH (Cy7.5-amine) loaded in A375 cells. $C_{\text{loading}} = 2 \mu\text{M}$, incubation time = 30 min, $\lambda_{\text{ex}} = 640 \text{ nm}$, $\lambda_{\text{em}} = 663\text{--}738 \text{ nm}$. Three fields of view (FOV) were recorded for each concentration, and 10 cells in average were recorded per FOV. Here representative cells are presented for each concentration. Scale bars = 25 μm . (b) Effect of the concentration of acetic acid in the population analysis of Cy7.5-amine-positive cells using flow cytometry. Cells to the right of the dotted line are considered Cy7.5-amine-positive. (c) Effect of the concentration of acetic acid on the population analysis of DAPI-permeabilized cells using flow cytometry. Cells to the right of the dotted line are considered cells permeabilized by DAPI. (d) Effect of the

concentration of acetic acid on the binding of Cy7.5-amine to the A375 cells using flow cytometry analysis for quantification. Average of two experiments is shown ($n = 2$). (e) Effect of the concentration of acetic acid on the percentage of DAPI permeabilized cells using flow cytometry analysis for quantification. Cells were treated with 2 μM Cy7.5-amine, incubated for 30 min, then were illuminated with 730 nm light at 80 mW cm^{-2} for 60 s. Since acetic acid protonates the phosphates in the phospholipids, the Cy7.5-amine binds less efficiently to lipid membranes. The lower binding of Cy7.5-amine to the cells is reflected in the lower permeabilization of the cells upon NIR light excitation. Average of two experiments is shown ($n = 2$). Detailed flow cytometry data processing is described in Supplementary Information Fig. 5.



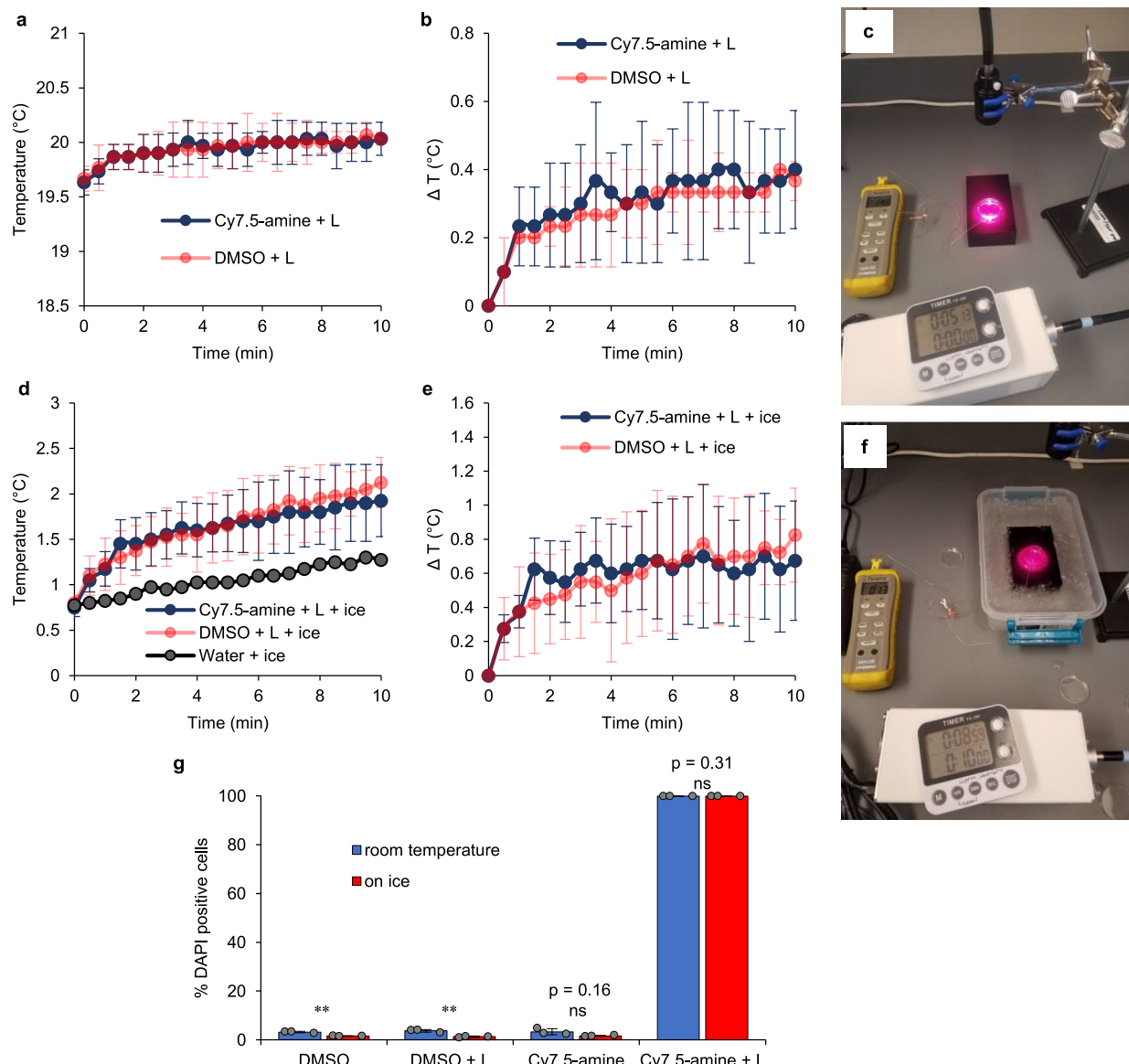
Extended Data Fig. 4 | Absorption spectrum of MJH and confocal fluorescence microscopy of A375 cells in the presence of MJH. (a) Absorption spectrum of MJH showing the position of the excitation lasers that were used in the confocal microscope ($\lambda_{\text{ex}} = 405 \text{ nm}$ with $\lambda_{\text{em}} = 425\text{--}475 \text{ nm}$ or $\lambda_{\text{ex}} = 640 \text{ nm}$ with $\lambda_{\text{em}} = 663\text{--}738 \text{ nm}$). (b) Expansion of the x and y axis of the absorption spectrum to observe the expected TMP (transversal molecular plasmon). The Cy7.5-amine shows a strong TMP (strong hybridization of longer C7 heptamethine bridge and larger benzoindole). Cy7-amine shows a weaker TMP and slightly shifted to $\sim 375 \text{ nm}$ because the C7 is hybridized to the smaller indole. Cy5.5-amine shows a strong TMP (larger benzoindole) but shifted to $\sim 360 \text{ nm}$ because of the hybridization with a weaker LMP (shorter C5 pentamethine). Cy5-amine shows little TMP because of the poor hybridization of the shorter C5 and smaller indole; this is the weakest combination because of the poor plasmonicity on both components. (c) Cells in the absence of dyes. (d) Cells in the presence of $2 \mu\text{M}$

Cy7.5-amine, 30 min of incubation. The emission of TMP mode can be observed at $\lambda_{\text{ex}} = 405 \text{ nm}$ in blue color. The excitation at 640 nm excites the tail of the LMP and produces a weak emission from Cy7.5-amine. (e) Cells in the presence of $2 \mu\text{M}$ Cy7-amine, 30 min of incubation. The emission from the LMP in Cy7-amine, since it is blue-shifted relative Cy7.5-amine, can be observed more intense in the red ($\lambda_{\text{em}} = 663\text{--}738 \text{ nm}$). (f) Cells in the presence of $2 \mu\text{M}$ Cy5.5-amine, 30 min of incubation. The emission from the LMP is clearly visible in red. (g) Cells in the presence of $2 \mu\text{M}$ Cy5-amine, 30 min of incubation. The emission from LPM is clearly visible in red. The emission from TMP (at $\lambda_{\text{ex}} = 405 \text{ nm}$) is not observed or is very weak in signal in e-g panel since the TMP is not present or shifted to other wavelengths on those molecules (Cy7, Cy5.5, and Cy5). For panels c-g, 75 cells in average were analyzed in each condition in the confocal microscope in 5 different locations. Two independent experiments were conducted. Here representative images are shown. Scale bars = $25 \mu\text{m}$.



Extended Data Fig. 5 | Excitation of the 680 nm vibronic shoulder in Cy7 improves the MJH effect for opening cell membranes in A375 cells. (a) Absorption spectra of Cy7-amine and overlaid with the spectral output of two LED lights: 730 nm and 680 nm. (b) Structure of Cy7-amine. (c) Flow cytometry analysis to measure the permeabilization of A375 cells in the presence of Cy7-amine without light. (d) Flow cytometry analysis to measure the permeabilization of A375 cells in the presence of Cy7-amine with 730 nm LED activation. (e) Flow cytometry analysis to measure the permeabilization of A375 cells in the presence of Cy7-amine with 680 nm LED activation. In all the flow

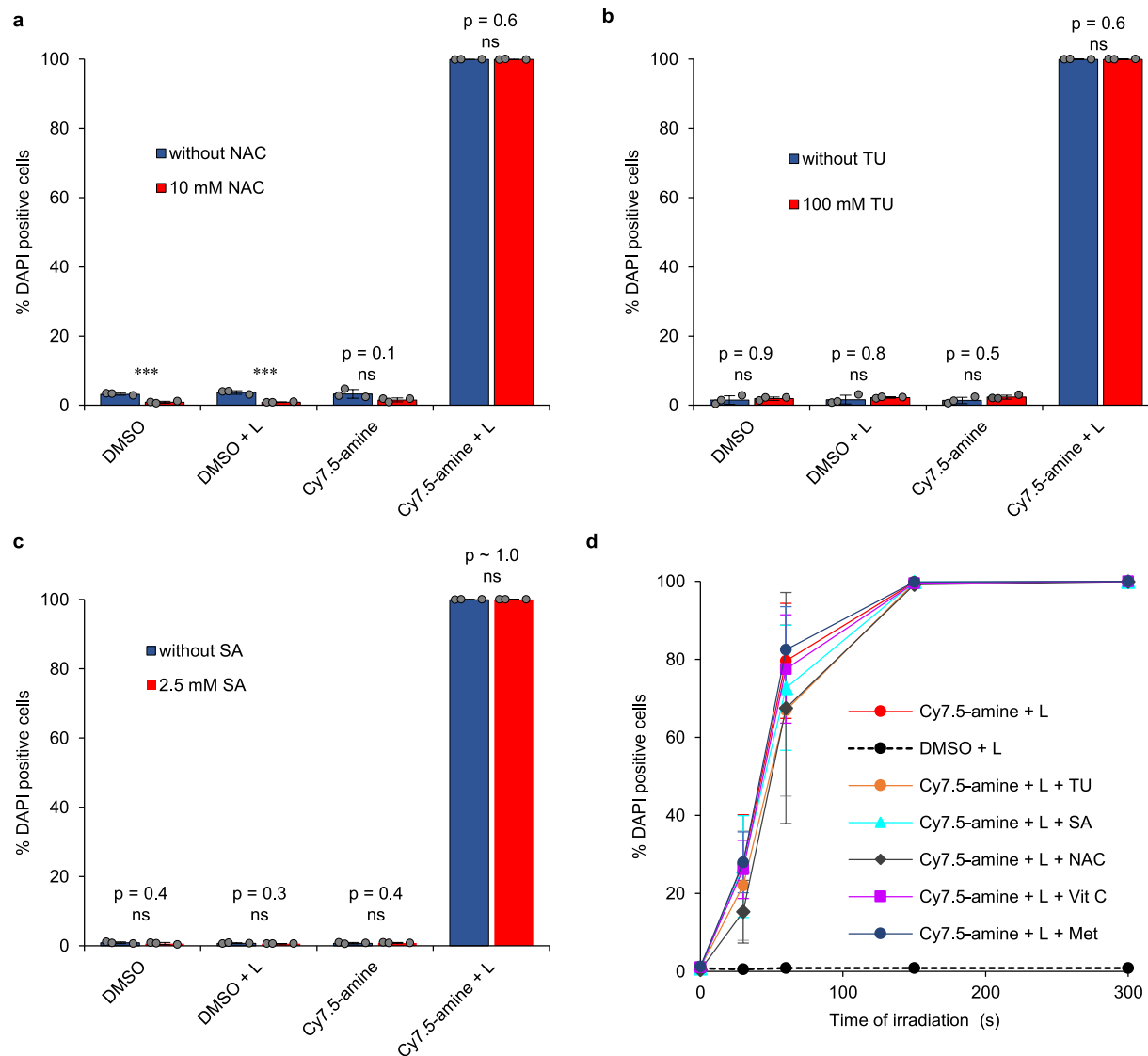
cytometry analyses the red line represents the gating to discriminate between DAPI negative and positive cells (permeable). In all the cases the incubation with the cyanine was for 30 min and irradiation was with an equal light dose of 80 mW cm^{-2} for 10 min. The light dose was calibrated with an Optical Power Meter from Thorlabs, sensor model S302C and console model PM100D. (f) Percentage of permeabilized cells, the numbers are obtained from the flow cytometry. 10,000 cells are analyzed per each concentration. Detailed flow cytometry data processing is described in Supplementary Information Fig. 5.



Extended Data Fig. 6 | Temperature of the cell suspension while under light treatment. Temperature on the cell killing experiment using Cy7.5-amine.

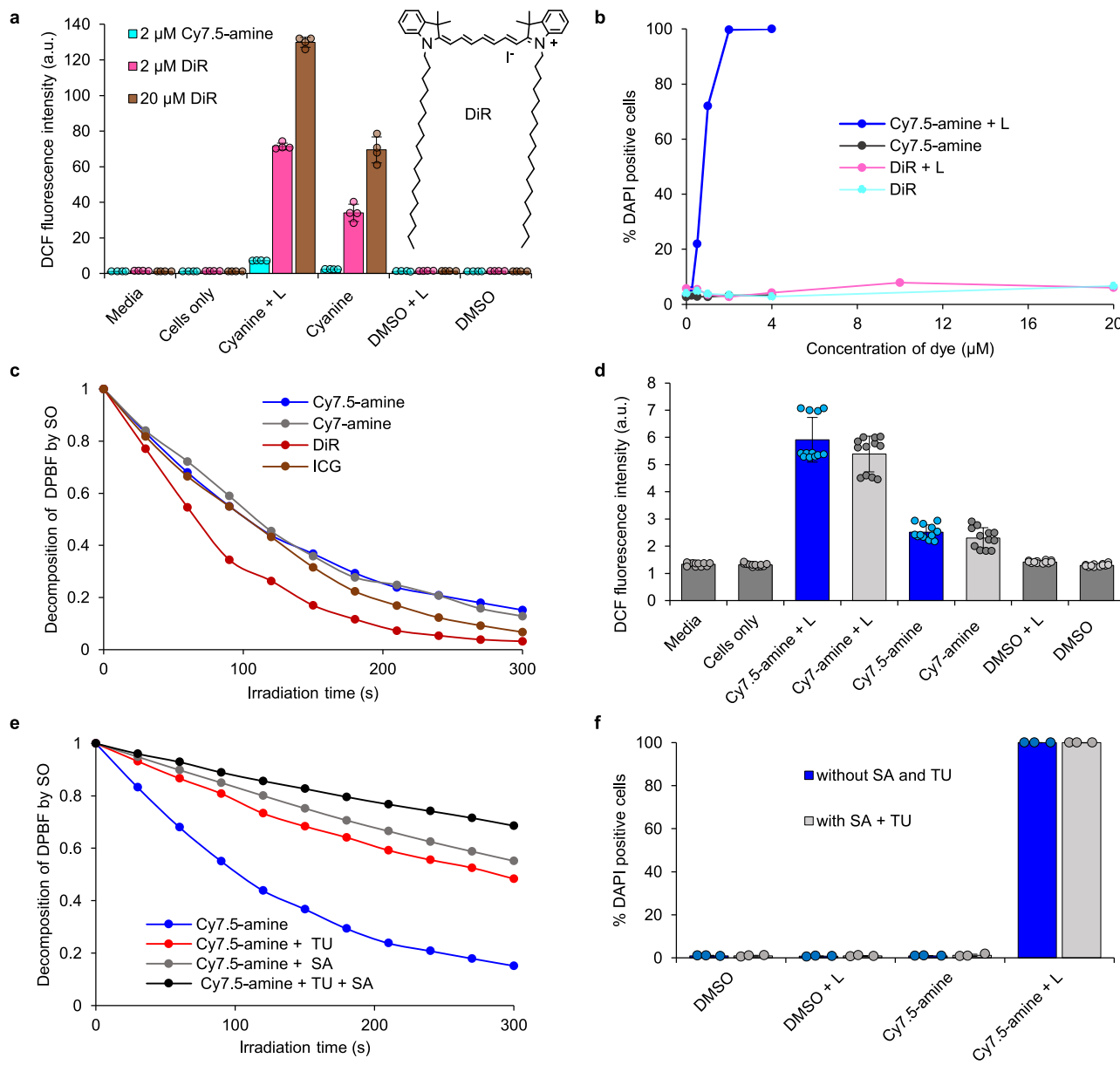
(**a-b, d-e**) No detection of heat production by Cy7.5-amine under NIR light treatment in the cell suspension (A375 cells) above the control. Temperature of the cell suspension (A375 cells) with 2 μ M Cy7.5-amine and under illumination with 730 nm NIR light (80 mW cm^{-2} for 10 min). The temperature of the media was recorded when the experiment was done at room temperature (**a-c**) and when the cell suspension was placed in an ice bath (**d-f**). A picture of the experimental set up when done at room temperature is shown in **c** and in ice bath is shown in **f**. In **d** ‘water + ice’ is the increase of the temperature because of the melting of ice without irradiation. In **e** the change of temperature is corrected by subtracting the temperature increase due to the melting of ice without illumination. The temperature of the cell suspension treated with NIR light and without Cy7.5-amine (DMSO + NIR light) correlates well with temperature profile in the suspension treated with NIR light containing 2 μ M Cy7.5-amine (Cy7.5 + NIR

light). There is no photothermal effect of Cy7.5-amine beyond the minimal heating caused by the light alone of $\sim 0.5^\circ\text{C}$. (**g**) Percentage of cells permeabilized to DAPI when the treatment was done at room temperature versus when was done placing the cell suspension on ice bath. Detailed flow cytometry data processing is described in Supplementary Information Fig. 5. *t*-test, two-tail, * $p < 0.05$, ** $p < 0.01$, *** $p < 0.001$. Statistical significance $p < 0.05$, ns = not significant. The exact p values obtained were 0.0036 (**), 0.006 (**), 0.16 (ns), 0.31 (ns) when comparing the permeabilization at room temperature versus in ice bath for the DMSO, DMSO + L, Cy7.5-amine, and Cy7.5-amine+L groups, respectively. In **a** and **b** 3 independent samples were processed and measured ($n = 3$). In **d** and **e** 4 independent samples were processed and measured ($n = 4$). In **g** 3 independent samples were processed and measured by flow cytometry ($n = 3$). In all, the data are presented as mean values \pm SD, respectively. For ‘water + ice’ control in panel **d** data as mean values are presented ($n = 4$).



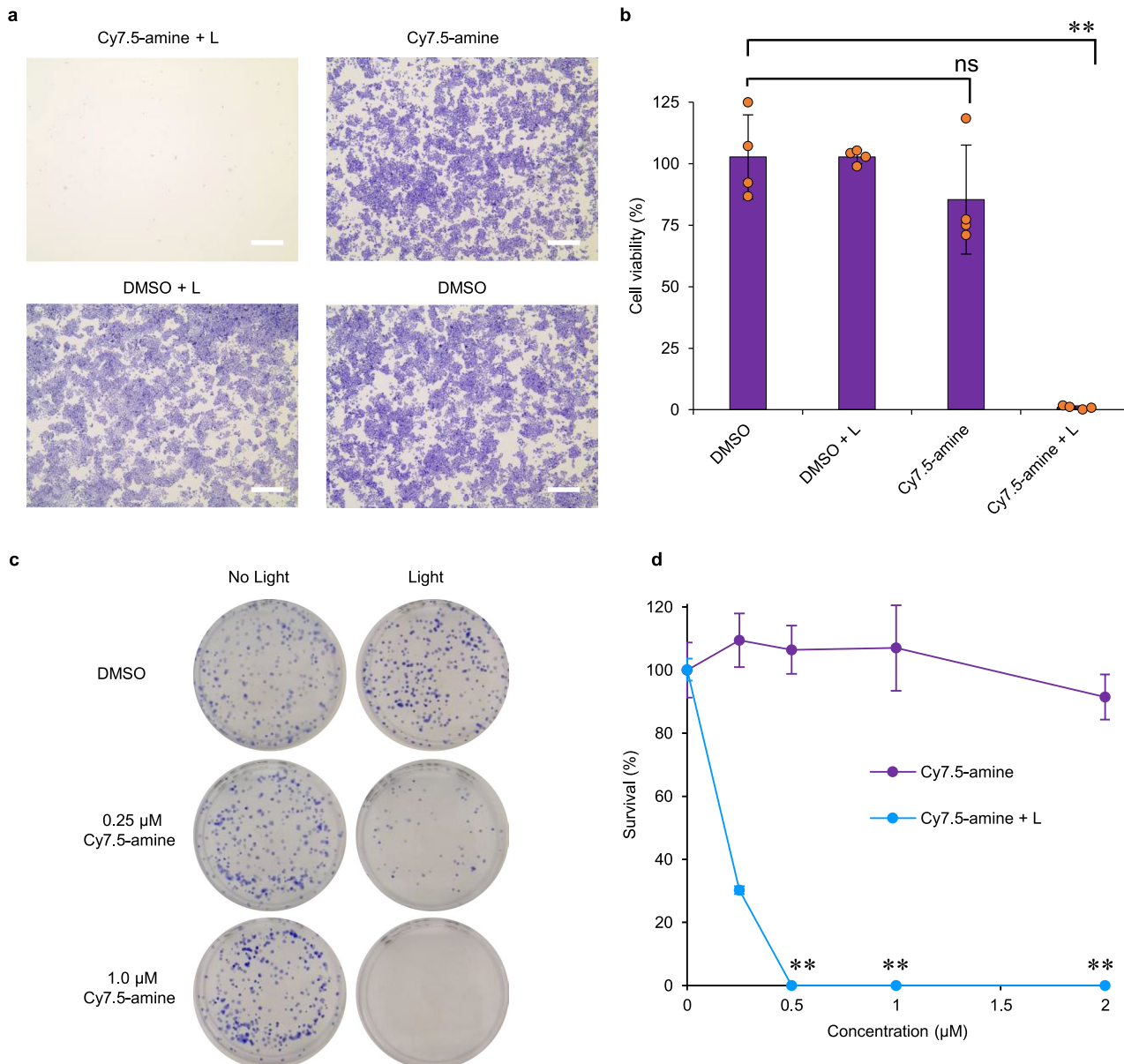
Extended Data Fig. 7 | ROS effects on the cell killing using Cy7.5-amine. ROS scavengers do not retard the permeabilization of A375 cells to DAPI when treated with 2 μ M Cy7.5-amine under illumination with 730 nm NIR light (80 mW cm $^{-2}$ for 10 min). (a) Effect of 10 mM NAC (*N*-acetylcysteine). The exact p values obtained were 0.0004, 0.0005, 0.0969 and 0.6005 for the DMSO, DMSO + L, Cy7.5-amine, and Cy7.5-amine+L groups, respectively. (b) Effect of 100 mM TU (thiourea). The exact p values obtained were 0.9071, 0.8021, 0.4631, and 0.5918 for the DMSO, DMSO + L, Cy7.5-amine, and Cy7.5-amine+L groups, respectively. (c) Effect of 2.5 mM SA (sodium azide). The exact p values obtained were 0.3712, 0.2751, 0.4267, and 1.0 for the DMSO, DMSO + L, Cy7.5-amine, and Cy7.5-amine+L groups, respectively. (d) Effect of ROS scavengers at variable irradiation time of 730 nm NIR light at 80 mW cm $^{-2}$. Five different scavengers were used: TU 100 mM,

azide 2.5 mM, NAC 1 mM, Vit C (vitamin C) 5 mM and Met (methionine) 5 mM. DMSO control contains 0.1% DMSO in the media because DMSO is used to pre-solubilize the Cy7.5-amine stock solution at 2 mM and diluted to 1:1000 to obtain 2 μ M Cy7.5-amine in media containing 0.1% DMSO. Experimental groups are: DMSO = 0.1% DMSO, DMSO + L = 0.1% DMSO + NIR light treatment, Cy7.5 = 2 μ M Cy7.5-amine and Cy7.5 + L = 2 μ M Cy7.5-amine + NIR light treatment. In all the plots 3 independent samples were processed and analyzed by flow cytometry (n = 3). In all plots data are presented as mean values \pm SD, respectively. t-test, two-tail, *p < 0.05, **p < 0.01, ***p < 0.001 Statistical significance p < 0.05, ns = not significant. Detailed flow cytometry data processing is described in Supplementary Information Fig. 5.



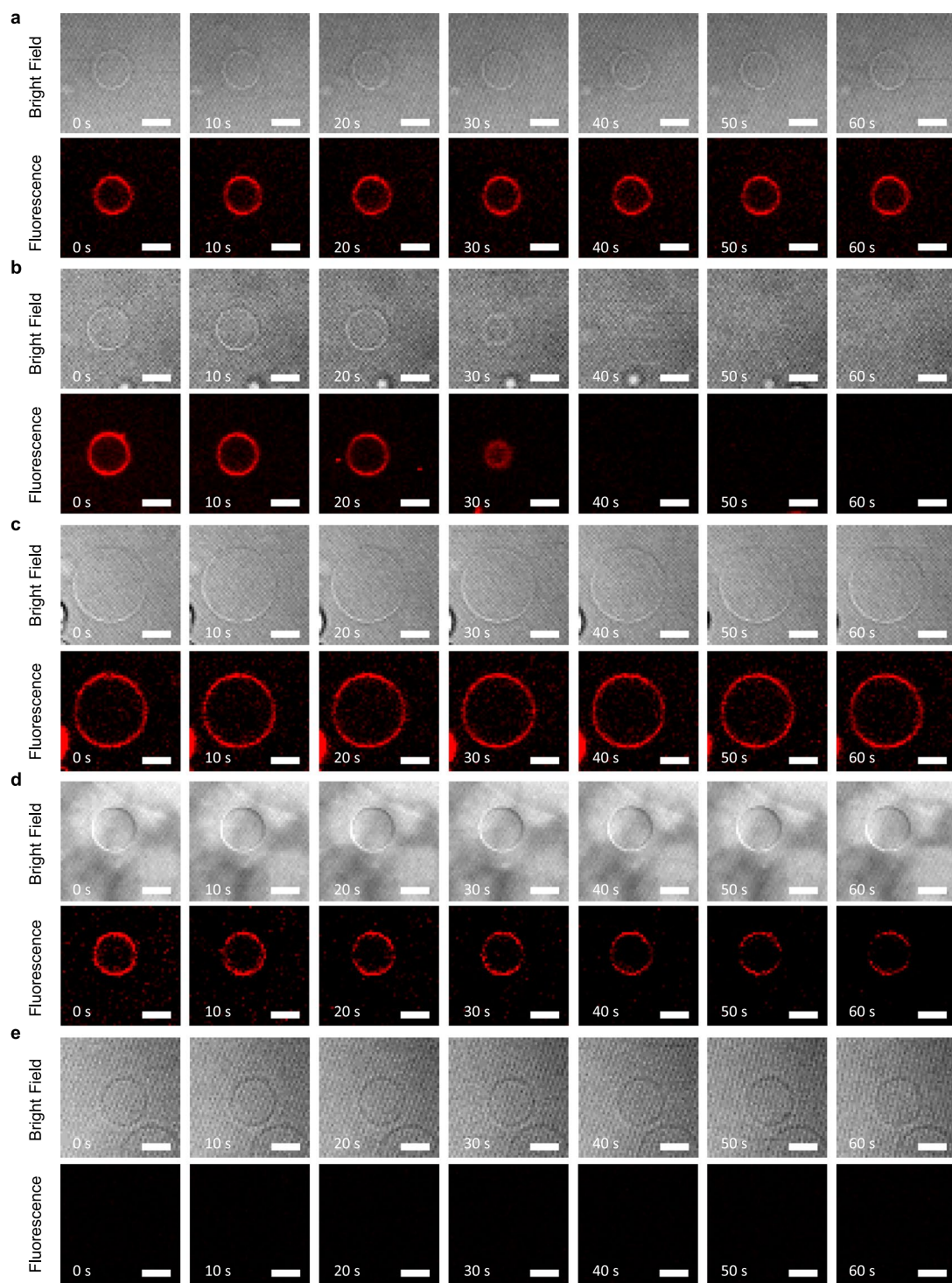
Extended Data Fig. 8 | Quantification of ROS and singlet oxygen (SO) levels and their effect on the cell killing using Cy7.5-amine versus the cell-membrane-targeting DiR dye (a strong photosensitizer control). (a) Measurement of ROS levels in A375 cell suspensions using 2,7'-dichlorodihydrofluorescein diacetate as the ROS probe in the presence of 2 μ M Cy7.5-amine versus 2 μ M DiR and 20 μ M DiR with and without light (L). The number of samples processed and measured were n = 4. (b) Percentage of DAPI positive cells as a function of the concentration quantified from the flow cytometry analysis. DiR that produced 10–20-fold more ROS than Cy7.5-amine did not permeabilize the A375 cells. This continues to support that the DiR structure is a weaker MJH with poorer VDA (See Extended Data Fig. 2). And more importantly, that ROS is not responsible for the permeabilization of DAPI into the cells. 5,000 cells were analyzed by flow cytometry for each concentration (n = 1). (c) Quantification of SO levels by the decomposition rate of DPBF (1,3-diphenylisobenzofuran) under light illumination in the presence of four cyanine dyes: 2.6 μ M Cy7.5-amine, 2.6 μ M Cy7-amine, 2.6 μ M DiR and 2.6 μ M ICG. DiR and ICG produces more SO than Cy7.5-amine or Cy7-amine yet DiR was unable to permeabilize the cells (number of samples n = 1). (d) ROS levels in cells

in the presence of Cy7.5-amine versus Cy7-amine. Cy7.5-amine and Cy7-amine produced approximately the same levels of SO and ROS yet Cy7.5-amine is a much stronger MJH in cell permeabilization (Fig. 2). The number of samples processed and analyzed were n = 12. (e) Shutting down the levels of SO generation by adding thiourea (TU = 100 mM) or sodium azide (SA = 2.5 mM) or a combination of TU 100 mM and SA 2.5 mM into the 2 μ M Cy7.5-amine solution under LED illumination (number of samples n = 1). (f) Effect of ROS scavenger combo (100 mM TU and 2.5 mM SA) on the percentage of DAPI positive cells as quantified from the flow cytometry analysis in the presence of 2 μ M Cy7.5-amine with and without illumination: no difference observed in the cell permeabilization to DAPI (number of samples n = 3). Unless otherwise specified, the light irradiations doses were 80 $mW\ cm^{-2}$ for 10 min using a 730 nm LED. Except, in b the LED light (L) was a 740 nm light from Keber Applied Research Inc. at the same dose of 80 $mW\ cm^{-2}$ for 10 min. This was done with a different LED because the data was collected in the early stage of the research, and we later moved to use the 730 nm LED for all the experiments. In all, the data are presented as mean values, and the error bars are the standard deviations, respectively. For panel c and f, detailed flow cytometry data processing is described in s.



Extended Data Fig. 9 | Quantification of cell death by crystal violet assay and clonogenic assay. A375 cells treated with Cy7.5-amine and 80 mW cm⁻² of 730 nm NIR light for 10 min. (a) Representative microscopy picture of each condition in the crystal violet assay ($n = 4$). Experimental groups consist of: Cy7.5-amine + L = 2 µM Cy7.5-amine + 80 mW cm⁻² of 730 nm NIR light for 10 min; Cy7.5-amine = 2 µM Cy7.5-amine; DMSO + L = 0.1% DMSO + 80 mW cm⁻² of 730 nm NIR light for 10 min; and DMSO = 0.1% DMSO. Scale bar = 0.5 mm. (b) Crystal violet assay. Plot showing the quantification of the cell viability from the absorbance of crystal violet. Sample repetitions $n = 4$ for each condition in a 24 well plate (independent samples). Data are presented as mean values \pm SD. *t*-test, two-tail, * $p < 0.05$, ** $p < 0.01$, *** $p < 0.001$. Statistical significance $p < 0.05$. The exact p values obtained were $p = 0.0012$ (**) and $p = 0.26$ (ns), respectively. (c) Clonogenic assay. Representative pictures showing the growth of cell colonies in the controls (0.1% DMSO with or without light) and complete eradication of A375 cells when treated with 1 µM Cy7.5-amine + light (80 mW cm⁻² of 730 nm NIR light for 10 min). (d) Clonogenic assay. Quantification of the number cells forming colonies. The survival is the percentage of cells that formed colonies. The results are normalized relative to the DMSO control. Sample repetitions $n = 3$ (independent samples). Data are presented as mean values \pm SD. *t*-test, two-tail, * $p < 0.05$, ** $p < 0.01$, *** $p < 0.001$. Statistical significance $p < 0.05$. The exact p values obtained were $p = 0.002$ (at 0.5 µM), $p = 0.005$ (at 1 µM) and $p = 0.002$ (at 2 µM).

obtained were $p = 0.0012$ (**) and $p = 0.26$ (ns), respectively. (c) Clonogenic assay. Representative pictures showing the growth of cell colonies in the controls (0.1% DMSO with or without light) and complete eradication of A375 cells when treated with 1 µM Cy7.5-amine + light (80 mW cm⁻² of 730 nm NIR light for 10 min). (d) Clonogenic assay. Quantification of the number cells forming colonies. The survival is the percentage of cells that formed colonies. The results are normalized relative to the DMSO control. Sample repetitions $n = 3$ (independent samples). Data are presented as mean values \pm SD. *t*-test, two-tail, * $p < 0.05$, ** $p < 0.01$, *** $p < 0.001$. Statistical significance $p < 0.05$. The exact p values obtained were $p = 0.002$ (at 0.5 µM), $p = 0.005$ (at 1 µM) and $p = 0.002$ (at 2 µM).



Extended Data Fig. 10 | Time-course treatment of DPhPC GUVs with MJHs and under VDA photoactivation. A strong MJH (Cy5.5-amine) is compared against a weak MJH (Cys-amine). The photoactivation consisted of continuous exposure to 640 nm confocal microscope laser at 5% power (50 μ W power, Plan Apo IR 60x/1.27 water immersion objective). Fluorescence images are recorded by imaging at $\lambda_{\text{ex}} = 640 \text{ nm}$, $\lambda_{\text{em}} = 663\text{--}738 \text{ nm}$, and 5% (50 μ W) laser power every 10 s.

a) DPhPC GUV treated with 2 μ M Cy5.5-amine without VDA photoactivation.
b) DPhPC GUV treated with 2 μ M Cy5.5-amine and under VDA photoactivation.
c) DPhPC GUV treated with 2 μ M Cys-amine without VDA photoactivation.
d) DPhPC GUV treated with 2 μ M Cys-amine and under VDA photoactivation.
e) DPhPC GUV treated with 0.1% DMSO as control and under photoactivation.
The pictures were recorded every 10 s for all the panels. Scale bar 5 μ m.

Reporting Summary

Nature Portfolio wishes to improve the reproducibility of the work that we publish. This form provides structure for consistency and transparency in reporting. For further information on Nature Portfolio policies, see our [Editorial Policies](#) and the [Editorial Policy Checklist](#).

Statistics

For all statistical analyses, confirm that the following items are present in the figure legend, table legend, main text, or Methods section.

n/a Confirmed

- The exact sample size (n) for each experimental group/condition, given as a discrete number and unit of measurement
- A statement on whether measurements were taken from distinct samples or whether the same sample was measured repeatedly
- The statistical test(s) used AND whether they are one- or two-sided
Only common tests should be described solely by name; describe more complex techniques in the Methods section.
- A description of all covariates tested
- A description of any assumptions or corrections, such as tests of normality and adjustment for multiple comparisons
- A full description of the statistical parameters including central tendency (e.g. means) or other basic estimates (e.g. regression coefficient) AND variation (e.g. standard deviation) or associated estimates of uncertainty (e.g. confidence intervals)
- For null hypothesis testing, the test statistic (e.g. F , t , r) with confidence intervals, effect sizes, degrees of freedom and P value noted
Give P values as exact values whenever suitable.
- For Bayesian analysis, information on the choice of priors and Markov chain Monte Carlo settings
- For hierarchical and complex designs, identification of the appropriate level for tests and full reporting of outcomes
- Estimates of effect sizes (e.g. Cohen's d , Pearson's r), indicating how they were calculated

Our web collection on [statistics for biologists](#) contains articles on many of the points above.

Software and code

Policy information about [availability of computer code](#)

Data collection

LE-MA900 FP-Cell Sorter Software (SONY) for flow cytometry data collection
Tecan i-control 2.0 software (TECAN, Austria) for 96 well plate reader absorbance and fluorescence.
NIS-Elements Imaging Software (NIKON) for confocal microscopy data collection.

Data analysis

LE-MA900 FP-Cell Sorter Software (SONY) for flow cytometry data collection and analysis.
FlowJo 10.5.3 for flow cytometry data analysis and plotting of final flow cytometry plots.
NIS-Elements AR5.21.03 Imaging Software (NIKON) for confocal microscopy data collection and analysis.
ImageJ 1.52a (National Institute of Health, USA) public software for counting number of forming colonies in the clonogenic assay.
Microsoft Office Home and Student 2016 (excel and power point) for data analysis and figures.
Perkin Elmer ChemDraw Professional 16.0 for drawing chemical structures.
VESTA version 3.5.7 for three-dimensional visualization of electronic chemical structures.

For manuscripts utilizing custom algorithms or software that are central to the research but not yet described in published literature, software must be made available to editors and reviewers. We strongly encourage code deposition in a community repository (e.g. GitHub). See the Nature Portfolio [guidelines for submitting code & software](#) for further information.

Data

Policy information about [availability of data](#)

All manuscripts must include a [data availability statement](#). This statement should provide the following information, where applicable:

- Accession codes, unique identifiers, or web links for publicly available datasets
- A description of any restrictions on data availability
- For clinical datasets or third party data, please ensure that the statement adheres to our [policy](#)

The source data used during this study are uploaded to the Zenodo database, accessible at: <https://doi.org/10.5281/zenodo.8271482>. The datasets generated during and/or analyzed during the current study are available from the corresponding author on request.

Human research participants

Policy information about [studies involving human research participants and Sex and Gender in Research](#).

Reporting on sex and gender

NA

Population characteristics

NA

Recruitment

NA

Ethics oversight

NA

Note that full information on the approval of the study protocol must also be provided in the manuscript.

Field-specific reporting

Please select the one below that is the best fit for your research. If you are not sure, read the appropriate sections before making your selection.

Life sciences

Behavioural & social sciences

Ecological, evolutionary & environmental sciences

For a reference copy of the document with all sections, see nature.com/documents/nr-reporting-summary-flat.pdf

Life sciences study design

All studies must disclose on these points even when the disclosure is negative.

Sample size

Sample size calculation was performed. Expected mean differences between the control and the treatment group and expected standard deviations were obtained from previous tumor growth delay experiments in our research group. For therapeutic significance, in the B16-F10 tumor model we expected to observe a mean value of the tumor size in the control group at 400 mm³ and standard deviation of 220 mm³ versus a mean value of 50 mm³ and standard deviation of 50 mm³ in the treatment group. Selecting a power of 80% (probability of finding an effect) and two-tailed significance level of 5% ($p = 0.05$, confidence interval = 95%), we calculated 4 mice per group. Considering 10% of attrition factor (death/euthanasia due to ulcerations, moribund, other reasons) during the study, then we placed DMSO+Light (n=5), Cy7.5-amine+Light (n=5, one was deceased during the study, n=4 final) and Cy7.5-amine (n=4). The attrition factor for correcting mice numbers was justified since we have observed attrition in previous studies using light activated molecular machines (MM) in the MM+Light treatment group in B16-F10 model possibly by a triggered strong immune-and-anti-inflammatory response. No attrition was expected in the control group treated with Cy7.5-amine based on previous preliminary experiments, then n=4 was justified. For therapeutic significance, in the A375 tumor model study we increased the significance level (two-tailed, $p = 0.001$, confidence interval = 99.9%) and power of 90%. The expected mean values in the control group were 400 mm³ and standard deviation of 220 mm² versus 50 mm³ and standard deviation of 50 mm³ in the treatment group. Using these parameters, we predicted 9 mice per group. Then correcting by 10% of attrition factor. Then we placed 10 mice per group.

Data exclusions

No data was excluded

Replication

The flow cytometry analyses were repeated multiple times ($n = 3$ or larger) at a single concentration and the results were reproducible. Then, when the concentration response curves were measured, one sample was analyzed per concentration, but 7 or more concentrations were analyzed per molecule. The flow cytometry analysis were very reproducible even when the experiments were done on different repetitions on different days. Sometimes in flow cytometry a baseline of high cell death population was presented, but we learn to fix that by washing the culture plate several times with PBS buffer to wash off any dead cell (which typically easily detach) and then harvest the healthy cells only, with this trick we got typically ~98-99% viable cell population measured using DAPI at the beginning of the treatments. The ROS measurement were very reproducible, even when the experiments were done at different repetitions on different days. The temperature measurements on the media varied relatively depending on the temperature of the room, so I have to do these measurements on the same day for better reproducibility since the temperature exchange in the solution will depend on the room temperature. In this way have similar initial temperatures at time zero of irradiation. The singlet oxygen measurements using DPBF as a probe, it will be varied from the condition of DPBF, always fresh solution was prepared for

better reproducibility to avoid using long-stored-autoxidized BPBF in solution. And always fresh solution prepared of all compounds. Experiment on confocal microscopy photoactivation of molecular jackhammers (Fig. 4) was repeated in an independent experiment (several months later) and the result were reproducible.

In vivo, therapeutic efficacy study in F16-F10 tumor model was performed once (n=4 per group, this is 4 repetitions). But we justified change to work with A375 tumor model since B16-F10 produces high levels of melanin which interferes with the vibronic-driven-action photoactivation (written in the main text). Then A375 tumor model was conducted with a larger repetition number (n=10 mice per group). The therapeutic effect by VDA was successfully observed in both studies *in vivo*.

The binding of MJH into the A375 cells and the effect of acid in the media (lower pH) and its quantification (Extended Data Figure 3) was performed twice and the replications were successful (10,000 cells were analyzed).

Localization of molecular machines with confocal microscope (Extended Data Fig 4), two experiments were performed independently, the second experiment was performed several months later, and the results were successfully replicated.

The experiment of photoactivation of Cy7-amine using 680 nm Light versus 730 nm light (Extended Data Fig 5) was performed once. However, several concentrations were tested to measure the concentration response and 10,000 cells were analyzed per each concentration.

The effects of ROS scavengers on the cell permeabilization (Extended Data Fig 6) were performed 3 times independently, and in all attempts the replication were successful.

Clonogenic assay and crystal violet assay were repeated 3 and 4 times independent samples, and in all the attempts the replications were successful.

The time-course VDA treatment of DPhPC GUVs were replicated n=7 independent experiments. Not every experiment was successful because it required localization of the GUVs immobilized on the PVA matrix. Such matrix likely was formed during the synthesis. This PVA matrix possibly is a mixture of free phospholipids and PVA. When the GUVs were immobilized and localized sitting on the surface of this matrix, the experiments were successful. When the GUVs were encapsulated too deep within the matrix it was more difficult to image them and it was more difficult to disassemble them due to the matrix physically could prevent them from breaking. In this last case, not every experiment was successful.

Randomization

Mice were randomly allocated. Mouse cages were allocated randomly, injected with tumor cells. Next, mice were randomly placed in new cages to reduce any cell injection bias per cage. For experiments other than animal experiments, the covariates were controlled by keeping covariates constant among experimental groups, for example: incubation temperature, time of incubation, times of exposure, room temperature (conduct the experiment at similar room temperatures for the time-course temperature measurements), times between sample preparation and measurement, prepare fresh samples of DPBF every time for the ROS experiment to avoid differences due to chemical decomposition, measure and calibrate the light doses frequently, etc.

Blinding

A staff investigator (AC) who was blinded to the group allocation performed the measurements and data collection. Other member of the team (RR) conducted the initial data analysis. And (CAO) finalized the data analysis and final plots. This approach reduced any bias to the expected results.

Reporting for specific materials, systems and methods

We require information from authors about some types of materials, experimental systems and methods used in many studies. Here, indicate whether each material, system or method listed is relevant to your study. If you are not sure if a list item applies to your research, read the appropriate section before selecting a response.

Materials & experimental systems

n/a	Involved in the study
<input checked="" type="checkbox"/>	<input type="checkbox"/> Antibodies
<input type="checkbox"/>	<input checked="" type="checkbox"/> Eukaryotic cell lines
<input checked="" type="checkbox"/>	<input type="checkbox"/> Palaeontology and archaeology
<input type="checkbox"/>	<input checked="" type="checkbox"/> Animals and other organisms
<input checked="" type="checkbox"/>	<input type="checkbox"/> Clinical data
<input checked="" type="checkbox"/>	<input type="checkbox"/> Dual use research of concern

Methods

n/a	Involved in the study
<input checked="" type="checkbox"/>	<input type="checkbox"/> ChIP-seq
<input type="checkbox"/>	<input checked="" type="checkbox"/> Flow cytometry
<input checked="" type="checkbox"/>	<input type="checkbox"/> MRI-based neuroimaging

Eukaryotic cell lines

Policy information about [cell lines and Sex and Gender in Research](#)

Cell line source(s)

Mouse melanoma B16-F10 cells were obtained from the ATCC (CRL-6475). Originally was isolated from skin tissue of a mouse with melanoma. B16F10 is a murine melanoma cell line from the C57BL/6J mouse. It is a subclone of the B16 tumor line, generated by injecting mice with B16 tumor cells, collecting and culturing secondary tumor growths, then injecting them into fresh mice, a total of 10 times. B16F10 cells are highly metastatic and can form tumors and metastases post implantation into syngenic C57BL/6 mice or immunocompromised mice.
Human melanoma A375 cells were obtained from ATCC (CRL-1619). Originally was isolated from the skin of a 54-year-old, female patient with malignant melanoma.

Authentication

ATCC source. Cell morphology coincided with the reported at ATCC and literature such as the expected rate of tumor growth and presence of melanin.

Mycoplasma contamination

ATCC source. Quality control specifications = mycoplasma no detected.

Commonly misidentified lines
(See [ICLAC](#) register)

Our cell lines F16-F10 and A375 were searched against commonly misidentified cell lines data base, <https://iclad.org/>/databases/cross-contaminations/ , and they were not found.

Animals and other research organisms

Policy information about [studies involving animals](#); [ARRIVE guidelines](#) recommended for reporting animal research, and [Sex and Gender in Research](#)

Laboratory animals

In our studies we used 7-8 weeks old female C57BL/6J mice (Jackson Laboratories, strain #000664) or 7-8 weeks old athymic female nude (nu/nu) mice from Envigo/Harlan labs. The housing conditions of the mouse were: Temperature 72 oF (high 74 oF, Low 70 oF), humidity 45% (high 55%, low 40%) and 12 h light/dark cycle.

Wild animals

Study did not involve wild animals

Reporting on sex

The murine B16F10 and human A345 melanoma cells generate tumors in male and female C57BL/6J mice and nude mice respectively. In this study we selected females because males tend to fight and sometimes, they injured their subcutaneous tumors, these will affect the outcome of our experiments.

Field-collected samples

The study did not involve samples collected from the field.

Ethics oversight

All animal studies were approved (protocol number 00000950-RN03) by the Institutional Animal Care and Use Committee (IACUC) of the University of Texas MD Anderson Cancer Center (Houston, TX).

Note that full information on the approval of the study protocol must also be provided in the manuscript.

Flow Cytometry

Plots

Confirm that:

- The axis labels state the marker and fluorochrome used (e.g. CD4-FITC).
- The axis scales are clearly visible. Include numbers along axes only for bottom left plot of group (a 'group' is an analysis of identical markers).
- All plots are contour plots with outliers or pseudocolor plots.
- A numerical value for number of cells or percentage (with statistics) is provided.

Methodology

Sample preparation

A375 cells were cultured as described in materials and methods. One day before the treatment, cells were inoculated at 5 million cells per dish (10 cm polystyrene tissue culture dish). The cells were harvested using 0.05% trypsin-EDTA (Gibco, 25-300-054), then the cells were counted and were adjusted to a cell density of 2x10⁵ cells/mL in DMEM media with L-glutamine, 4.5 g/L glucose, and sodium pyruvate (Corning Inc. 10013CV) and supplemented with 10% FBS (Corning, 35010CV), 1X MEM vitamin solution (Gibco, 11120052), 1X MEM non-essential amino acid solution (Gibco, 11140050) and penicillin/streptomycin. 1 mL of this cell suspension containing 2x10⁵ cells was used in each treatment. In a 1.5 mL Eppendorf tube, 1 µL of stock solution containing 2 mM Cy7.5-amine (or other cyanine molecule or other concentration) in DMSO (Fisher, 99.7%) was placed in the bottom of the tube, then 1 mL of the cell suspension was added into the tube to get final concentration of 2 µM of Cy7.5-amine containing 0.1% DMSO and 2x10⁵ cells. The mixture was then incubated at 37 °C and 5% CO₂ for 30 min. Then, 1 µM DAPI was added into the cell suspension. Then, the cells suspension was transferred to a 35 mL polystyrene tissue culture dish and immediately the cells were treated under the light beam of NIR light of 730 nm at 80 mW/cm² (or adjusted powers down to 20 mW/cm²) for 10 min (or adjusted illumination times down to 30 s) using LED light source (Prizmatix, UHP-F-730, Israel) which covers the entire dish. The spectral intensity of the LED is shown in Fig. 1e. While the cells were treated, the dish was placed on top of an aluminum block painted black, so that the excess NIR light and that was not reflected back into the cell suspension while the aluminum block acts as a heat-sink, maintaining a constant temperature in the dish during the irradiation. The instrument for flow cytometry analysis (SONY, MA900 Multi-Application Cell Sorter using the LE-MA900 FP-Cell Sorter Software) was already set up and calibrated by the time the light treatment was finished. Therefore, as soon as the 10-min light treatment was completed, the cell suspension was rapidly transferred from the 35 mm dish to a flow cytometry tube and the cells were analyzed for DAPI permeabilization and Cy7.5-amine binding. It took ~30 s to load the sample and to start the analysis. Therefore, the permeabilization of cells was measured as DAPI positive cells and occurred immediately due to the membrane permeabilization caused by Cy7.5-amine excitation with the 730 nm NIR light. The flow cytometry data was analyzed using FlowJo software. The light intensity was measured using an Optical Power Meter from Thorlabs, sensor model S302C and console model PM100D.

Instrument

SONY, MA900 Multi-Application Cell Sorter

Software

SONY, LE-MA900 FP-Cell Sorter Software

Cell population abundance

Typically the cell population of interest for the analysis was nearly ~95-99 %. This is the population of singlets within the cell population.

Gating strategy

Flow cytometry data processing and gating strategy. The flow cytometry data was analyzed using FlowJo software version

Gating strategy

10.5.3. The cells were plotted using the forward scattering area (FSC-A) versus side scattering area (SSC-A) as shown in Supplementary Information Fig. 5a. Then, a wide polygonal gate was drawn as shown in Supplementary Information Fig. 5a since we were interested to detect any cell death after treatment, we were not only interested to measure healthy cell populations. Sometimes, we observed that some dead cell population upon treatment could shift outside the gate if a narrow gate was used. Then, the singlet cells were selected by plotting the FSC-A versus the forward scattering height (FSC-H) as shown in Supplementary Information Fig. 5b. Then, the singlets were selected and the DAPI fluorescence intensity was plotted versus the SSC-A and the gate for DAPI positive cells was drawn as shown in Supplementary Information Fig. 5c and the analysis was applied to all samples in the group. In Supplementary Information Fig. 5d can be observed a DAPI positive population in the same analysis group. This analysis was applied to calculate the percentage of DAPI positive cells. The same gating analysis also was done in the SONY, LE-MA900 FP-Cell Sorter Software while collecting the data.

Tick this box to confirm that a figure exemplifying the gating strategy is provided in the Supplementary Information.